รายงานวิจัยฉบับสมบูรณ์

โครงการ การพัฒนาและปรับปรุงการตรวจจับออปติกดิสก์อัตโนมัติ

โดย ผศ. ดร. ภคินี เอมมณี

12 มิถุนายน 2560

กิตติกรรมประกาศ

ข้าพเจ้าขอขอบพระคุณหน่วยงานที่สำคัญหลายหน่วยงานดังต่อไปนี้ สำนักงานวิจัยแห่งชาติและมหาวิทยาลัยธรรมศาสตร์ที่ให้โอกาสในการรับทุนพัฒนานักวิจัยปี2557พร้อมทั้งให้เงินสนับสนุนโครงการวิจัยนี้ สถาบันเทคโนโลยีนานาชาติสิรินธรที่เอื้อเฟื้อสถานที่ทำงานและอุปกรณ์สำนักงานเครื่องใช้ที่จำเป็นทำให้ได้รับความสะดวกสบายตลอดการทำวิจัย ศูนย์ตาธรรมศาสตร์ที่ให้การสนับสนุนด้านข้อมูลรูปภาพถ่ายจอประสาทตา ความช่วยเหลือในการจัดหาคำตอบจากจักษุแพทย์เพื่อใช้เทียบผลจากอัลกอริทึม

นอกจากนี้โครงการนี้จะไม่สามารถสำเร็จได้หากไม่มีความร่วมมือร่วมใจและกำลังใจจากบุคคลดังต่อไปนี้ ผู้ร่วมทีมวิจัยซึ่งประกอบด้วย น.ส นิตยา เมืองนาคซึ่งเป็นนักศึกษาปริญญาเอกของข้าพเจ้าที่ลงแรงเขียนโปรแกรมจนสำเร็จตามแผนงาน และ ศาสตราจารย์ ดร. สแตนิสลาฟ มากานอฟ ที่เป็นทั้งเพื่อนร่วมทีมวิจัยและที่ปรึกษาที่คอยช่วยแนะแนวทางการทำวิจัยและแก้ไขปัญหาต่างๆตลอดการทำวิจัยจนกระทั่งโครงการนี้สำเร็จลุล่วงไปได้ด้วยดี ขอขอบคุณ ผศ.ดร. สนติพีร์ เอมมณี ที่คอยรับฟังปัญหาและคอยเป็นกำลังใจที่ดีตลอดมา ท้ายที่สุดนี้ ข้าพเจ้าหวังเป็นอย่างยิ่งว่างานวิจัยนี้นี้จะเป็นประโยชน์กับนักวิจัยท่านอื่นๆที่สนใจงานด้านนี้และงานวิจัยจะได้นำไปประยุกต์ใช้จริงในโปรแกรมช่วยเหลือทางการแพทย์ในอนาคต

ผศ.ดร.ภคินี เอมมณี

บทคัดย่อ

งานวิจัยนี้เสนอ 2 อัลกอริทึมที่มีชื่อว่า Vessel Transform(VT) และ Vessel Vector based Phase Portrait Analysis (VVPPA) ในการตรวจจับจานประสาทตาอัตโนมัติ ทั้งสองอัลกอริทึมที่มีความถูกต้องแม่นยำสูงแม้ใช้ในภาพถ่ายจอประสาทตาที่คุณภาพแย่ ซึ่งทั้งสองอัลกอรทึมนี้ตรวจจับจานประสาทตาอัตโนมัติจากการใช้ข้อมูลของเส้นเลือดที่ปรากฏในรูปภาพถ่ายจอประสาทตาเป็นหลักแทนที่จะใช้คุณลักษณะเฉพาะของจานประสาทตาอย่างเดียว

วิธีVT หาตำแหน่งของจานประสาทตาอัตโนมัติโดยใช้หลักการว่า ตำแหน่งของจานประสาทตาเป็นตำแหน่งที่ผลรวมของระยะทางจากตำแหน่งนี้ไปแขนงเส้นเลือดหลักน้อยที่สุดเทียบเมื่อเทียบกับตำแหน่งอื่นๆบนรูป วิธีVVPPAเปลี่ยนเส้นเลือดหลักให้เป็นเวคเตอร์โดยใช้ข้อมูลจากเส้นเลือดเช่นมุมระหว่างเส้นเลือด ความหนา ความเข้ม เวคเตอร์จากเส้นเลือดจะนำไปพิจารณาร่วมกับเวคเตอร์ที่ได้จากเทคนิคอื่นๆ เพื่อหาจุดที่เวคเตอร์ทั้งระบบมาบรรจบจบรวมกัน

จากการทดลองจากเซตข้อมูลรูปภาพจอประสาทตา 2 เซตซึ่งแต่ละเซตแบ่งเป็นกลุ่มรูปที่คุณภาพดีและรูปที่คุณภาพไม่ดีพบว่าทั้งสองวิธีสามารถหาตำแหน่งของจานประสาทได้ดีกว่าวิธีอื่นที่นำมาเปรียบเทียบซึ่งก็คือFuzzy Convergence อย่างชัดเจนโดยเฉพาะอย่างยิ่งรูปในกลุ่มที่คุณภาพไม่ดี วิธีVT มีค่าความถูกต้องสูงกว่าวิธี Fuzzy Convergence มากถึง 32%ในบางเซตข้อมูล

Keywords: Vessel Transform(VT), Vessel Vector Based Phase Portrait Analysis (VVPPA), Optic disk localization.

Abstract

Two algorithms namely *Vessel Transform* (VT) and *Vessel Vector based Phase Portrait Analysis* (VVPPA) are proposed to automatically detect an optic disk (OD) in the retina images. They both yield high accuracy even when the quality of the images is poor. These algorithms utilize the features of vessels rather than the features of the ODs in the images.

The VT method localizes the optic disk using the concept that the location of the OD in a retina image is the point where the sum of the shortest distances from it to the major clusters of vessels is minimum compared to those from other locations. Whereas, VVPPA converts the main blood vessels into vectors using vessel features such as angle between vessels, thickness, and intensity and considers these vectors together with vectors derived from other techniques to find the location where all vectors converge to.

The images from each of the two collections are categorized into poor and fair subgroups. Both proposed methods yield noticeably better accuracy than compared a state-of-the art method which is Fuzzy Convergence method especial on images categorized as poor. The VT method outperforms Fuzzy Convergence up to 32%.

Keywords: Vessel Transform(VT), Vessel Vector Based Phase Portrait Analysis (VVPPA), Optic disk localization.

สัญญาเลขที่
RSA5780034

รายงานวิจัยฉบับสมบูรณ์

โครงการ พัฒนาและปรับปรุงการตรวจจับออปติกดิสก์อัตโนมัติ

ผศ. ดร. ภคินี เอมมณี
สถาบันเทคโนโลยีนานาชาติสิรินธร มหาวิทยาลัยธรรมศาสตร์

สนับสนุนโดยสำนักงานกองทุนสนับสนุนการวิจัย
และ มหาวิทยาลัยธรรมศาสตร์

Project Code: RSA5780034

(รหัสโครงการ)

Project Title: The Development and Improvement of Automatic Optic Disc Detection

(ชื่อโครงการ) การพัฒนาและปรับปรุงการตรวจจับออปติกดิสก์อัตโนมัติ

Investigator: Asst. Prof. Dr. Pakinee Aimmanee

(ชื่อนักวิจัย) ผศ. ดร. ภคินี เอมมณี

E-mail Address: pakinee@siit.tu.ac.th

Project Period: 16 June 2014 - 15 June 2017

(ระยะเวลาโครงการ) 16 มิถุนายน 2557 - 15 มิถุนายน 2560

Vessel Transform for Automatic Optic Disk Detection in Retinal Images

Nittaya Muangnak, Pakinee Aimmanee, Stanislav Makhanov, Bunyarit Uyyanonvara

nittaya2mua@gmail.com, pakinee@siit.tu.ac.th, makhanov@siit.tu.ac.th, bunyarit@siit.tu.ac.th,

Sirindhorn International Institute of Technology

Thammasat University

131 Moo 5, Tiwanont Road, Bangkadi, Muang, Pathumthani 12000, Thailand

1. Introduction

Precise automatic localization of an optic disk (OD) in the retinal images is an important problem in the ophthalmic image processing. Once the OD has been identified, many other regions of clinical importance such as the fovea or macula can be easily detected and/or localized. The OD is also important for establishing a frame of reference within the retinal image. The OD usually appears in the retinal images as a bright, yellowish, circular or oval object, roughly one-sixth the width of the image in diameter [2]. Any irregularity in the appearance of the OD is a sign of abnormalities or diseases such as glaucoma, diabetic retinopathy (DR) or hypertensive retinopathy [3] [4].

Nowadays, one in ten people is advised for annual retinal screening due to a variety of medical conditions [7]. However, annual retinal screening is nearly impossible especially in developing countries due to the huge gap between the number of professional ophthalmologists and the patients. This implies the necessity of automatic screening systems to assist the ophthalmologists in diagnosing the early stage of diseases such as glaucoma and diabetic retinopathy using computer-based identification. Since the eye fundus imaging is a frequent clinical procedure, the retinal images are commonly be used for a preliminary diagnosis and detecting suspicious cases.

Early works assume that the OD is the largest cluster of bright pixels. Therefore, the conventional OD segmentation approaches often employ a suitable set of features such as brightness, shape, size, and the variation of the gray level (entropy) [11][12]. Numerous work is based on these features, for instance, template matching [17][18], boundary tracing [19], active contours (snakes) [13][21]-[23], machine learning [12], [26], [27], multilevel thresholding [28], shape detection [29], mathematical morphology [N1][N2][N3], PCA [N8], genetic algorithms [N9] edge-based detection [32] and blood vessel tracing [33][34], a pyramidal decomposition and Hausdorff-based template matching guided by scale tracking of large objects using a multi-resolution image decomposition [17], edge detection combined with a boundary tracing [19], a k-Nearest Neighbor regression with a circular template [35], and circular transformation [N4].

For example, Lalonde et al. assumed OD is one of the brightest areas. They localized the OD by using a pyramidal decomposition where the pyramid is created using a simple Haar-based discrete wavelet transform with the set high pass and low pass filters, then segmented the OD using a Hausdorff-based template matching[17]. Li and Chutatape localized the OD by using principal component analysis (PCA) then detected the OD's boundary using an iterative searching procedure to find the modeled objects so called active shaped model (ASM) [25]. Lowell et al. performed the optic disk localization using specialized template matching, and segmentation by using an active contour (snake) [16]. Lu et al. employed two important features of OD which are brightness and texture's smoothness to form a model template to localize the OD, approximated OD region is approximately determined by a pair of morphological operations, refined an ellipse that is fitted by the convex hull of the detected OD region. Akram and Kham employed the intensity variation and the gray levels as the major features characterizing the OD [14].

One of the most successful work which provides the result comparisons with many existing approaches is the work of Lu proposed in 2011. Curvelet transform has also been applied to solve the OD segmentation problem [N11, N12, N15]. It mathematically designed for contrast enhancement. Esmaeili et al. [N11] [N12] and Shahbeig et al. [N15] applied it to the image to easier locate the OD. Shahbeig et al. used it after preprocessed the image with PCA then used morphological operators based on geodesic conversions to obtain the OD region. Similarly, Esmaeili

et al. Pereira et al. used the existence of brightness on series of applied a famous Ant Colony Optimization (ACO) algorithm preceded by anisotropic diffusion for optic disc detection

Lu [N4] proposed an OD detection and segmentation based on the Circular Transform which is claimed to be more efficient, more accurate and faster than other state-of-the-art methods at that time [N5][N6][N7][N8]. In his method, after preprocessed the image he first localized the OD based on a probability map constructed from image gradient and image intensity in the horizontal and vertical directions [N7], and then applied the circular transformation to detect the shape of the OD. He reported the accuracy 98.24% which outperformed other approaches such as the work of [N5][N6][N7][N8].

A major drawback of approaches depending on OD features including the Lu's Circular Transformation approach is that it often incorrectly localizes the OD when the OD's physical appearance such as shape, color, brightness, or size becomes abnormal. The OD obscured by blood vessels or only partially visible (blur, shadows, noise) could be misclassified. Besides, the feature based methods could be highly sensitive to distracters such as yellow/white lesions or bright artifacts which often appear on the retinal images [15] [16].

A powerful subclass of the OD detection algorithms based on the location of the vascular structures is often overlooked. Only a few papers exploit the convergence of the blood vessels to the OD. Akita et al. [34] trace the parent-child relationship between blood vessels segments, tracking back to the center of the OD. In addition to brightness and shape feature of the OD, Chaudhuri et al. [36] check the area where vertically oriented vessels converge. The vessels are treated as a single line of an infinite length. Consequently, the detection of the convergence area has been reduced to the line intersection problem. Foracchia et al. [33] used the fact that all retina vessels originate from the OD and their paths follow a similar directional pattern (parabolic course).

To describe the general direction of retinal vessels at any given position in the image, a geometrical parametric model was proposed, where two of the model parameters are the coordinates of the OD center. The parameters are identified by an optimization algorithm.

One of the most successful vessel convergence techniques is introduced by Hoover and Goldbaum [2]. The method employing the vessel convergence as the primary feature is based on the fuzzy convergence [38] endowed with a voting scheme. The voting takes place on the integer grid of the original image. Each vessel is represented by a fuzzy segment, whose area contributes votes to its pixels. The summation of votes at each pixel produces an image map representing the strength of the convergence of each pixel. The map is then blurred and thresholded to produce points of the strongest convergence. The fuzzy convergence techniques have been applied on multiple scales and combined with a feature based approach employing the equalized brightness. The verification of the method on STARE database shows the highest performance overall (89%), and a complete success on the healthy retina test cases (100%). Nonetheless, the method does not consider the hierarchical structure of the vessels and their importance. As a matter of fact, the vessel network consists of the main vessels and several levels of secondary vessels (tributes to the main vessel). The main vessels converge to the OD whereas the secondary vessels are positioned randomly with regard to the OD. Therefore, the vascular network can be thought of as a collection of clusters of connected conduits similar to the river networks. The clusters converge to the OD in the sense that points belonging to the OD are closer to each cluster than points not belonging to OD. This concept is not always true if we consider convergence of individual vessels. It is not hard to give an example where the secondary vessels converge to a false OD. In addition, the cluster could be generated by a single main vessel and its binary rooted tree. It can also include several major vessel trees positioned closely and directed towards the OD.

To locate the convergence area of the vessels, we propose a procedure to decompose the vessels into clusters and then find the centroid of the points of which the distances from each point to all vessel clusters is the minimum. Our method is named Vessel Transform (VT). The VT algorithm has been tested retinal images from two standard databases against the fuzzy convergence method [38]. The OD location obtained from the VT is combined together with the scale space method [44] to detect the OD's rim. The numerical experiments demonstrate that the proposed algorithm outperforms the scale space method without VT in terms of the correct detection of the OD.

2. Vessel Transform

The vessel transform (VT) is given by

$$V(p) = \frac{1}{N}\sum_{i=1}^{N} \mathrm{dist}(p, c_i), \quad (1)$$

where c_i is the *i*-th cluster of vessels, *N* is the number of clusters, $p = (x, y)$ an arbitrary point in the image and $\mathrm{dist}(p, c) = \min_{p' \in c} \| p - p' \|$. An introductory example in Figure 1 displays sample retinal images and the corresponding VTs. The dark part of the VT image corresponding to the vessel convergence region locates the OD.

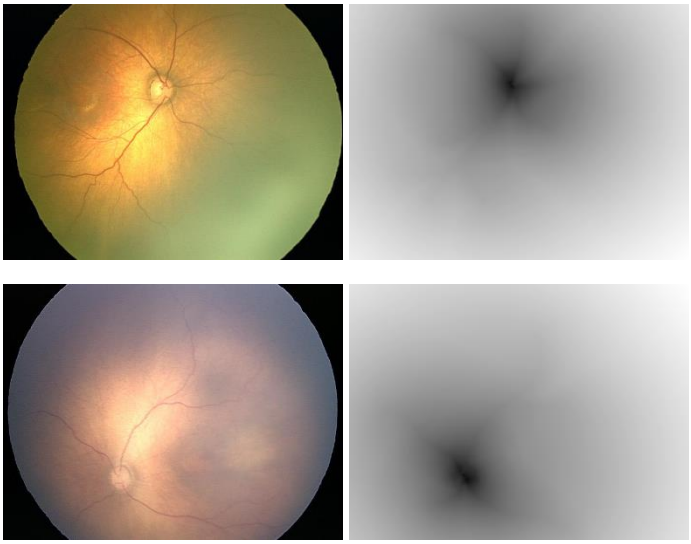

Figure 1 The original retinal images (left) and their corresponding VTs (right).

In order to apply the VT, the vessels in the original image are detected and extracted. However, breaking a single vessel into several segments is a common drawback produced by the majority of the vessel extraction algorithms [59], [60], [61]. Therefore, our clustering algorithm not only collects the vessels into clusters, but repairs individual broken vessels as well. The input of the clustering algorithm is a collection of vessels $(v_1, v_2, ...v_m)$. Each vessel is represented by the Cartesian coordinates: $v_i = ((x, y)_{i,1}, .(x, y)_{i,2}, ..., (x, y)_{i,N_i})$. We use a vessel segmentation freeware [62], [63] based on thresholding of wavelet coefficients on different spatial scales and a vessel location refinement using the centerline spline fitting.

The first step of our algorithm is preprocessing designed to remove the outliers: short, thin, and faint vessels. It requires the following thresholds: T_l-the length threshold, T_t - the thickness threshold, T_f - the threshold on the gray level intensity of the vessel relative to the background. The second step merges the vessels into clusters and removes the isolated vessels. The merging step employs a threshold T_d on the maximum distance between clusters which can be merged into a new cluster. We apply a classical hierarchical bottom-up clustering. Initially the algorithm treats each vessel as a singleton $c_i = v_i$. Next, it successively merges clusters c_i, c_j if $dist(c_i, c_j) < T_d$ until they have been merged into several well separated sets. The post processing procedure detects and removes the outliers (small clusters) by using the condition $N_{c_i} < T_L$, where N_{c_i} denotes the size of the cluster and T_L the corresponding threshold.

Note that this type of clustering does not include time consuming tracing procedures designed to detect the tree-like structures of the vessels. However, if trained, the algorithm returns well separated clusters sufficient to generate a VT which localizes the convergence region and consequently the OD. Figure2 illustrates the proposed clustering method.

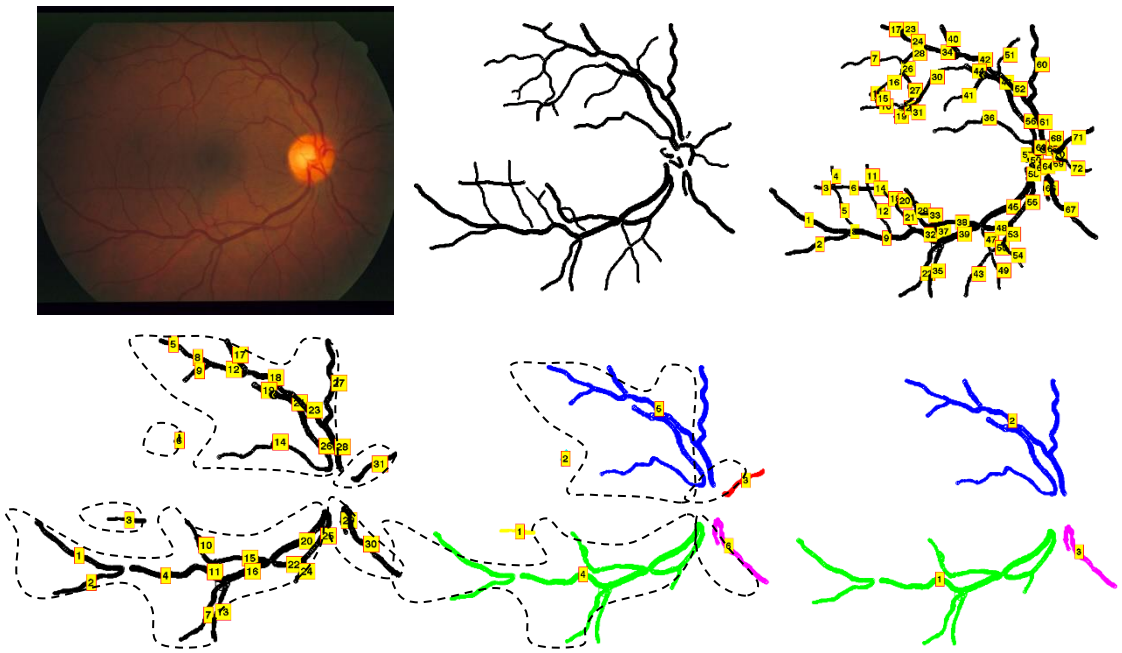

Figure 2 The original image (top left), extracted vessels (top right), segmented vessels (middle left), removing short, thin or faint vessels (middle right), clustering (bottom left), removing small clusters (bottom right).

3. Correction Algorithm

The VT based segmentation of the OD requires that the resulting clusters converge to the OD. Therefore, for the images merged into 3 or more clusters, we verify the quality of convergence as follows. First, we evaluate the convergence region $\Omega = \arg\min_{p} V(p)$ and its centroid. Next, we withdraw the clusters one by one from the collection of clusters and evaluate the convergence regions Ω' corresponding to these new collections. If for some Ω', $dist(\mathrm{O}_{\Omega}, \mathrm{O}_{\Omega'}) > T_{\Omega}$, where O_{Ω} is the centroid of Ω, O'_{Ω} the centroid of Ω' and T_{Ω} the corresponding threshold, the clustering is discarded. Our assumption is that if the vessels strongly converge to Ω, the system without one cluster converges approximately to the same region (see Figure 4). The second step is the evaluation of the convergence as follows:

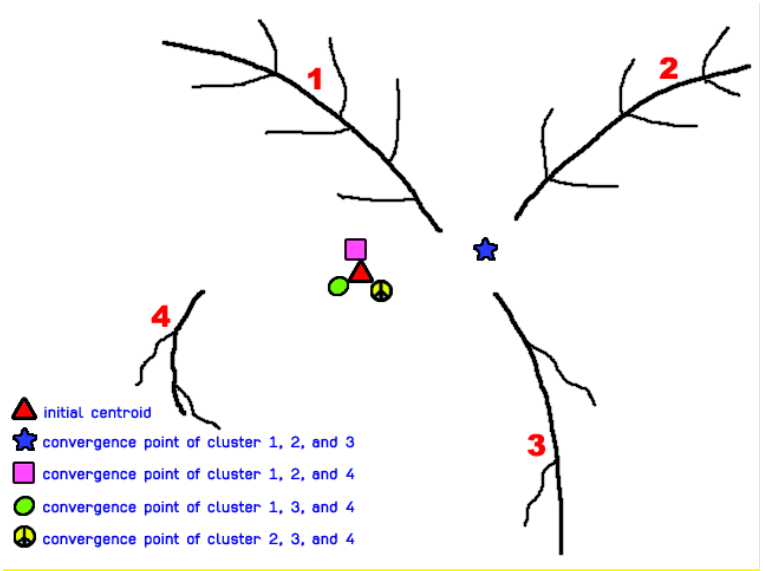

Figure 3 Convergence test

If $\min_{c_i}(dist(c_i,\Omega)) < T_{VT}$, where T_{VT} is the corresponding threshold and c_i the i^{th} cluster (the cluster is close enough to the convergence region). The clustering is considered successful if the centroid O_Ω of the convergence region Ω is located inside the OD. In this case, the VT is included in the prescribed set of features for a further evaluation.

In a few cases the clustering algorithm returns an unacceptable result which consists of only one or two clusters. In this case we could not reliably test the convergence by excluding clusters (the first step). Technically, one can modify the thresholds and merge the vessels into a new set of clusters. However, testing an algorithm based on this idea is still an open problem. Therefore, following [54] we discard the VT feature and apply the scale space algorithm in its original version [44] (see also our forthcoming chapter 6). The numerical experiments show that the number of the discarded images is usually small and does not exceed 10%. Besides, the location of the OD in these images can still be correctly evaluated.

4. Training Method

The method requires the following thresholds: T_l - the minimal acceptable length of the vessel for a particular image (shorter vessels will be eliminated), T_t - the minimal acceptable thickness, T_f - the maximum acceptable intensity of the vessel relative to the background, T_d - the maximum distance between the clusters which can be merged into a new cluster, T_L - the minimum acceptable size of the cluster, T_Ω and T_{VT} the thresholds used in the convergence test (see section 3). The algorithm is trained using the bivariate quadratic approximation given by

$$T(\mu,\sigma) = a_1\mu^2 + a_2\sigma^2 + a_3\mu + a_4\sigma + a_5\mu\sigma + a_6, \quad (2)$$

where μ and σ is the mean and the standard deviation of the corresponding parameter evaluated for a particular image. For instance, $T_l \equiv T_l(\mu_l,\sigma_l)$ is the threshold on the minimal acceptable length of the vessel, whereas μ_l is the mean length of a vessel in a particular image and σ_l the standard deviation.

5. Scale Space Algorithm with Vessel Transform (SSVT)

The VT method and its additional improvement schemes described in sections 2, 3, and 4 yields the approximated location of the OD but it hasn't yet detected the boundary of the OD. To get the OD's rim, we combine our approach with the scale space (SS) algorithm proposed by Duanggate et al [44]. The modified algorithm is called the space scale algorithm with the vessel transform (SSVT). Figure 4 shows how SS is combined with VT.

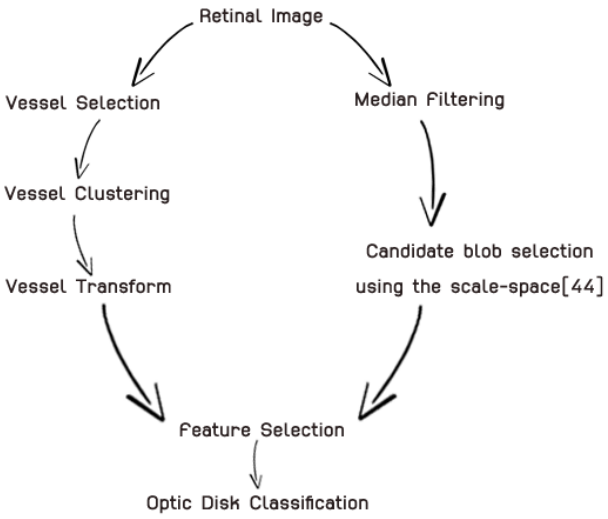

Figure 4 Vessel transform combined with the scale-space segmentation

The SS approach is based on the original theory proposed by Lindeberg [67] in 1994. The image is converted into a one-parameter family of smoothed images. Objects (blobs) which appear stable under smoothing at different scales along with their features are considered as the OD candidates. The features considered in [44] are the size, compactness (roundness), entropy and intensity. We extend the SS algorithm by adding the VT score as an additional feature. Our OD classification is performed using a decision tree which includes the above mentioned features along with the VT-feature.

6. Experimental Setup

We tested the proposed method against the existing techniques on two collections of images i.e. STARE (the STructured Analysis of the Retina) [53] and ROP [44]. The ROP was originally collected to detect the signs of retinopathy of prematurity by Dr. Sarah Barman with Kingston University of UK. Images with bright, round, and clear border of the ODs were classified visually as "fair", the rest is considered "poor". There are 60 images with fair quality and 31 images with poor quality for the ROP collection whereas 31 images with fair quality and 50 images with poor quality for the STARE collection. Figure 4-a and Figure 4-b display examples of "fair" and "poor" images.

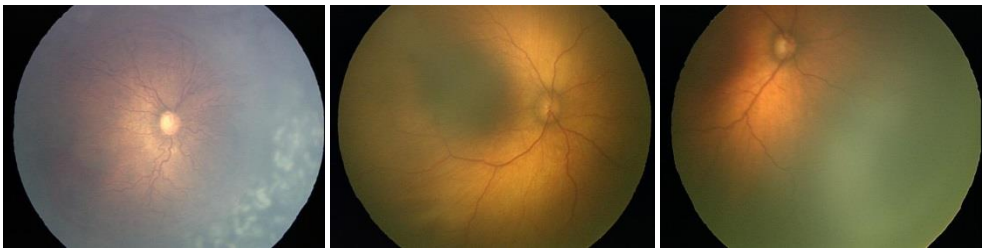

(a) Fair images

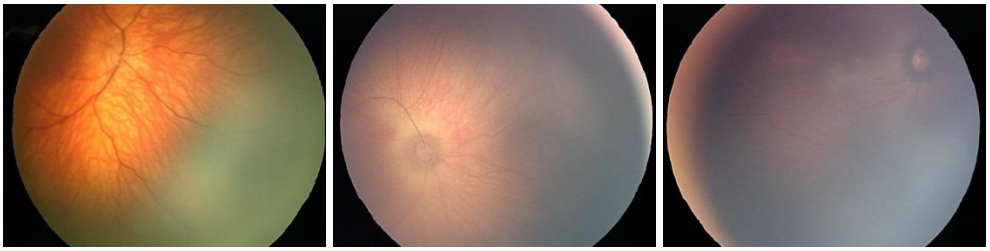

(b) Poor images

Figure 4 Examples of "fair" and "poor" images

Our two collections of test images have been obtained by different devices with different lighting conditions. Therefore, they require different sets of thresholds which are obtained by the quadratic regression (2). Figure 5 illustrates the threshold selection applied to the ROP and the STARE set, respectively. We train the method using the classic 70-30% ratio between the training and the testing data.

To combine features in scale space method, we use an automatic decision tree generation available from the Waikato Environment for Knowledge Analysis [64]. Features evaluated for the candidate blob in Scaled Space are the size (*s)*, the compactness (*c)*, the entropy (*e)*, the average intensity (*i)*, and the average value of the vessel transform (*V)*. The resulting decision trees and the particular thresholds are shown in Figure 6.

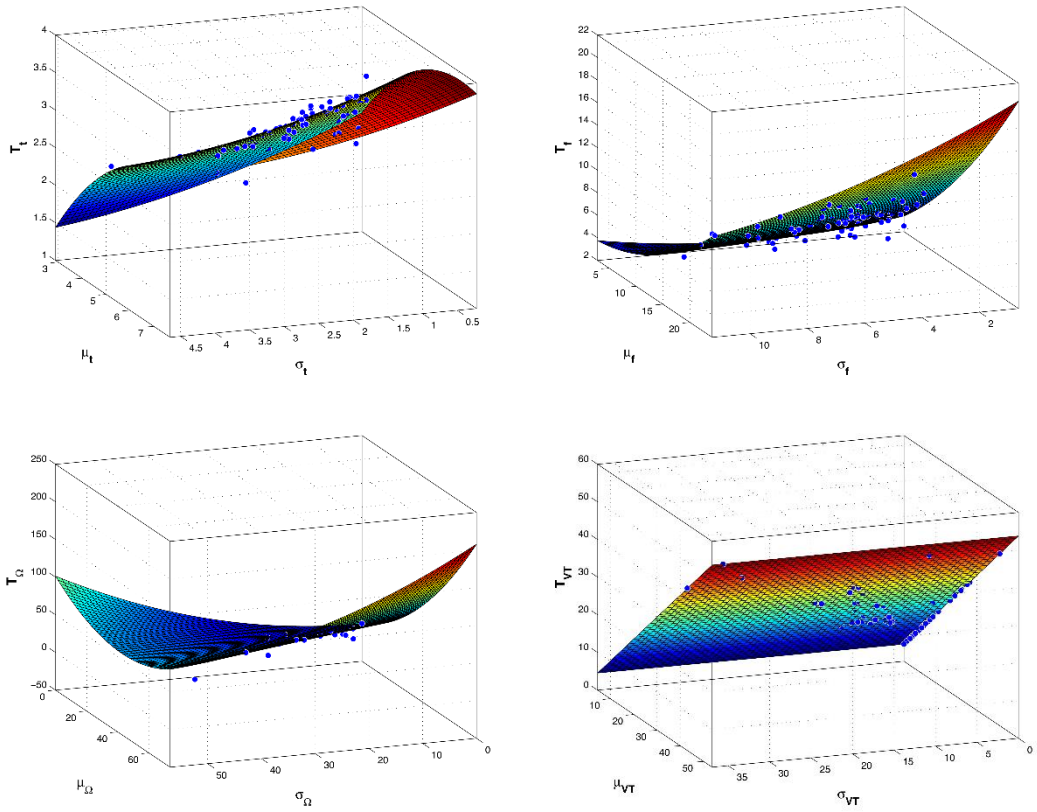

Figure 5 An example of Quadratic regressions for some parameters in the STARE collection

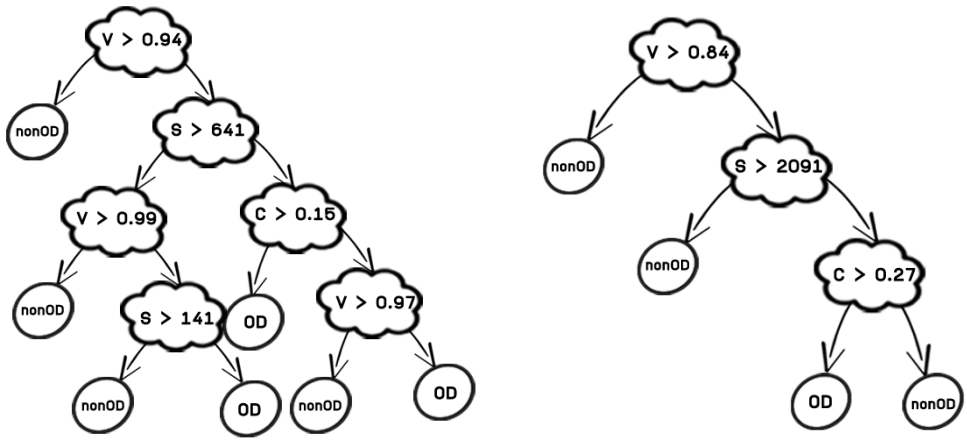

(a) The ROP collection (b) The STARE collection

Figure 6 The decision trees for test collections.

In the decision trees, we find that only V, s, and c play roles in detecting the OD region. Since they are independent of the entropy and the intensity, the new approach allows us to exclude the two features replacing them by the VT. Our forthcoming section 7 shows that the VT also improves the accuracy of the classification.

7. Experiments and Results

In this section, we show and analyze results of applying the proposed algorithm to the ROP and STARE collections of retinal images.

7.1 The Performance of the VT in Locating the OD

We applied and compared the performance of SSVT with the Scale Space Approach [46] and the Fuzzy Convergence Method (FC) [2]. Figure 10 shows introductory examples of locating the OD obtained by the VT and FC.

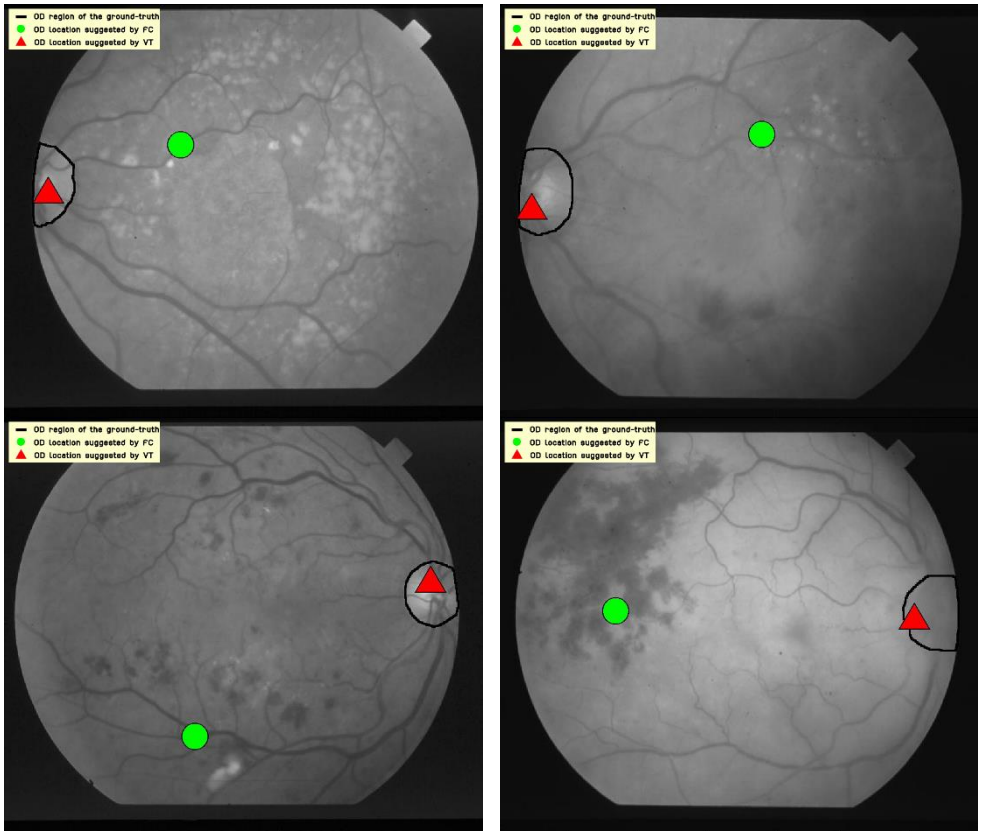

Figure 7 The OD locations produced by the VT and the FC

Figure 10 demonstrates some cases when the VT outperforms the FC owing to the vessel clustering approach which improves the accuracy of the locating the convergence region.

The accuracy of locating the OD was evaluated as follows. If the convergence region Ω (see section 3) is contained entirely inside the ground truth contour, we consider it a correct location of the OD.

Table 3 shows the accuracy of the location of the OD location for the poor and fair images processed by the VT and the FC on the STARE collection. The VT outperforms FC for the both groups with the absolute improvement of about 6%. The OD is considered to be located correctly if the centroid of the convergence region

Note that the results of applying the original FC to the STARE collections are taken from [55], however, they are not available for the ROP.

Table 3 Accuracy of OD location from Fuzzy Convergent and Vessel Transform

Collections	Image Quality	Accuracy (%)		Absolute Improvement VT vs. FC
		FC	VT	
ROP	Fair	N/A	95.00	N/A
	Poor	N/A	96.77	N/A
STARE	Fair	90.32	96.77	6.45
	Poor	88.00	94.00	6.00
Overall average (STARE only)		89.16	95.39	6.23

7.2 The Performance of the SSVT in Detecting the OD Region

This section presents the performance of SSVT vs. SS. As opposed to the previous section where the location of the OD was evaluated by finding the centroid of the convergence area, the OD region is determined by using a combination of the SS which generates the candidate blobs and the proposed decision tree based on the VT which is one of the most prominent features.

We evaluate the performance using two standard schemes: sensitivity and predictive Positive Value (PPV). The first one reveals the accuracy while the second one reflects completeness of the obtained solution. In this work, the sensitivity is defined to be the ratio of the number of pixels detected correctly as OD to the total number of pixels detected as OD. The PPV in this work is the ratio of number of pixels detected correctly as OD to the total number of pixels of OD from the ground truth.

The algorithms were tested on the ROP and the STARE collections. The experiments clearly demonstrate the advantage of SSVT. Figure 8 shows examples when the final selection of the SS fails whereas the SSVT decision tree points to the correct OD region. As a matter of fact, the VT-feature has a strong impact on the blob classification process. In many cases, the SS fails to detect the OD due to insufficient information provided by the basic features. As opposed to that, SSVT employs the convergence of the vessels which is not sensitive to the variation of the contrast and the noise as long as the entire vascular network or at least a major part of it has been correctly detected and clustered.

The tests of the performance of the SSVT against the SS are presented in Table 4. The performance measures are the average sensitivity and positive predictive value (PPV). The SSVT outperforms SS in *both quality measures for each group of the images (fair and poor) and for each collection of data.* In particular, when the image quality is poor, the SSVT outperforms the SS in terms of PPV considerably. For the group of fair images, the advantage of the SSVT in average sensitivity is up to 4.69% (STARE) whereas for the poor images the improvement is about 14.35% (ROP). As far as the PPV is concerned, SSVT better than SS by 30.12% (ROP) on the poor collection and by 7.03% (STARE) on the fair collection. The average absolute improvement is 6.09% for the sensitivity and 13.54% for the PPV.

It should be noted that in [44] SS was found to be superior with regard to the OD segmentations based on the morphological operations and the Circular Hough Transform [56-58] applied to ROP. Therefore, the SSVT outperforms the above mentioned methods as well with a greater advantage. Still there are images where SSVT fails. Those images are usually characterized by unclear vascular networks combined with noise and shadows shaped similarly to the vessels.

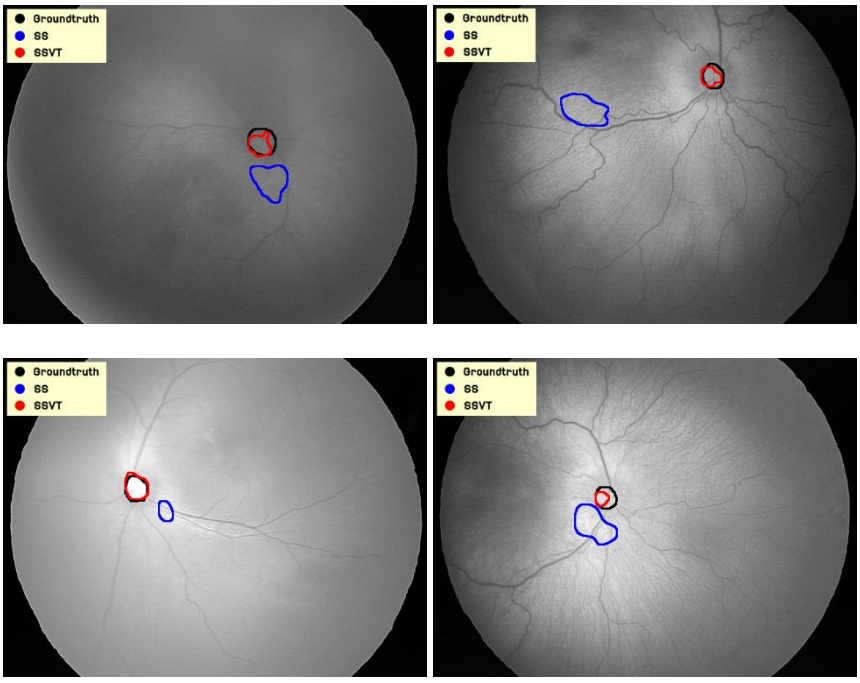

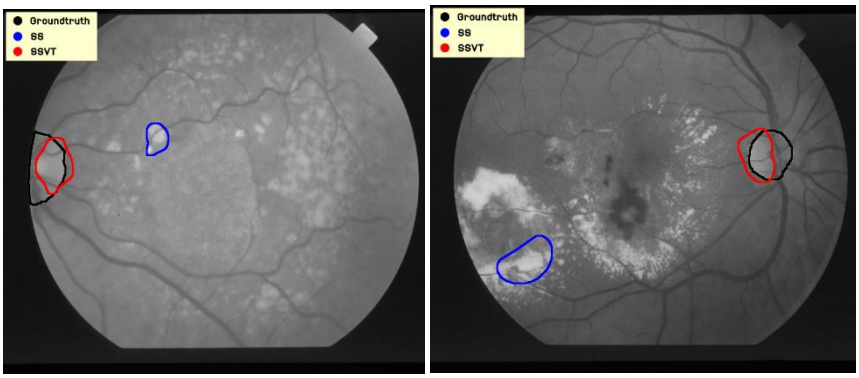

Figure 8 Examples of OD regions selected from SS (blue), SSVT (red) and the ground truth (GT) from 6 different images

Table 4 The Average Sensitivity and PPV of SS and SSVT for each image quality and each collection.

Collections	Image quality	Average Sensitivity		Average PPV	
		SS	SSVT (absolute improvement)	SS	SSVT (absolute improvement)
ROP	Fair	83.03	85.13 (+2.1)	83.41	84.67 (+1.26)
	Poor	47.60	61.95 (+14.35)	49.94	80.06(+30.12)
STARE	Fair	57.73	62.42 (+4.69)	67.61	74.64(+7.03)
	Poor	44.33	47.56 (+3.23)	56.82	72.56(+15.74)
Average		58.17	64.26 (+6.09)	64.44	77.98(+13.54)

8. Conclusions

The proposed new vessel transform improves the accuracy of locating the OD. The combination of the vessel transform with the feature based scale space segmentation improves the quality of the OD segmentation. The absolute improvement of the SSVT over SS measured in terms of sensitivity and positive predictive value is approximately 14 % and 30% respectively.

Acknowledgement

The authors would like to gratefully acknowledge financial support from Thailand Research Fund(TRF), grant number RSA5780034 and also Center of Excellence in Biomedical Engineering of Thammasat University.

References

[N1] S. Morales, V. Naranjo, J. Angulo, M. Alcaniz, Automatic Detection of Optic Disc Based on PCA and Mathematical Morphology, Medical Imaging, IEEE Transactions on , 32-4 (2013) 786-796

[N2] D. Welfer, J. Scharcanski, C. Kitamura, M. Pizzol, L. Ludwig, D. Marinho, Segmentation of the optic disk in color eye fundus images using an adaptive morphological approach, Computers in Biology and Medicine, 40-2 (2010) 124-137 .

[N3] D. Welfer, J. Scharcanski, D. Marinho, A morphologic two-stage approach for automated optic disk detection in color eye fundus images, Pattern Recognition Letters, 34-5(2013) 476-485.

[N4] S. Lu, Accurate and Efficient Optic Disc Detection and Segmentation by a Circular Transformation, IEEE Transactions on Medical Imaging, 30-12(2011), 2126-2133.

[N6] A. Youssif, A. Z. Ghalwash, and A. Ghoneim, "Optic disc detection from normalized digital fundus images by means of a vessels' direction matched filter," IEEE Transaction on Medical Imaging, 27- 1(2008) 11–18.

[N7] A. E. Mahfouz and A. S. Fahmy, "Ultrafast localization of the optic disc using dimensionality reduction of the search space," in Int. Conference Medical Image Computing Computer-Assisted Intervent., 2009, vol. 5762, pp. 985–992.

[N8] Carmona, E.J., Rincon, M., Garcia-Feijoo, J., Martinez-de-la-Casa, J.M.: "Identification of the optic nerve head with genetic algorithms", Artificial Intelligence in Medicine, 2008, vol.43, pp. 243-259

[N9] Dehghani, A., Moin, M.S., Saghafi, M.: "Localization of the optic disc center in retinal images based on the Harris corner detector", Biomedical Engineering Letters, 2012, vol. 2, no. 3, pp. 198-206

[N10] Dehghani, A., Moghaddam, H.A., Moin, M.S.: "Optic disc localization in retinal images using histogram matching", EURASIP Journal on Image and Video Processing, 2012, vol.19, pp. 1-13

[N11] Esmaeili, M., Rabbani, H., Dehnavi, A.M., Dehghani, A.: "Automatic detection of exudates and optic disk in retinal images using curvelet transform", IET Image Processing, 2012, vol. 6, issue 7, pp. 1005-1013

[N12] Esmaeili, M., Rabbani, H., Dehnavi, A.M.,: "Automatic optic disk boundary extraction by the use of curvelet transform and deformable variational level set model", Pattern Recognition, 2012, vol. 45, pp. 2832-2842

[N13] Hsiao, H.K., Liu, C.C., Yu, C.Y., Kuo, S.W., Yu, S.S.: "A novel optic disc detection scheme on retinal images", Expert Systems with Applications, 2012, vol.39, pp. 10600-10606

[N14] Mendonca, A.M., Sousa, A., Mendonca, L., Campilho, A.: "Automatic localization of the optic disc by combining vascular and intensity information", Computerized Medical Imaging and Graphics, 2013, vol. 37, pp. 409-417

[N15] Shahbeig, S., Hossein, P.: "Fast and automatic algorithm for optic disc extraction in retinal images using principle-component-analysis-based preprocessing and curvelet transform", Journal of Optical Society of America, 2013, vol. 30, no. 1, pp. 13-21

[N16] Pereira C., Goncalves, L., Ferreira, M.: "Optic disc detection in color fundus images using ant colony optimization" , Medical and Biological Engineering and Computing, 2013, vol.51, pp.295-303

[N17] Zhang, D., Zhao, Y.: "Novel accurate and fast optic disc detection in retinal images with vessel distribution and directional characteristics", IEEE Journal of Biomedical and Health Informatics, 2013, pp. 1-10

[N18] Morales, S., Naranjo, V., Angulo, J., Alcaniz, M.: "Automatic detection of optic disc based on PCA and mathematical morphology", IEEE Transactions on Medical Imaging, 2013, vol. 32, no. 4, pp.786-796

[N20] Ramakanth S.A., Babu, R.V.,: "Approximate nearest neighbor field based optic disk detection", Computerized Medical Imaging and Graphics, 2014, vol. 38, pp. 49-56

[N21] Pourreza-Shahri, R., Tavakoli, M., Kehtarnavaz, N.: "Computationally efficient optic nerve head detection in retinal fundus images", Biomedical Signal Processing and Control, 2014, vol. 11, pp. 63-73

[N22] Dashtbozorg, B., Mendonca, A.M., Campilho, A.: "Optic disc segmentation using the sliding band filter", Computers in Biology and Medicine, 2015, vol.56, pp. 1-12

[2] A. Hoover, M. Goldbaum, Locating the optic nerve in a retinal image using the fuzzy convergence of the blood vessels, IEEE Transactions on Medical Imaging 22-8(2003) 951-958.

[3] H. Li, O. Chutatape, Automated feature extraction in color retinal images by a model based approach, IEEE Transactions on Biomedical Engineering 51-2(2004) 246-254.

[6] S. Wild, G. Roglic, A. Green, R. Sicree, H. King, Global prevalence of diabetes: Estimates for the year 2000 and projections for 2030, Diabetes Care 27(2004) 1047–1053.

[8] S. Lu, J. Liu, J.H. Lim, Z. Zhang, N.M. Tan, W.K. Wong, T.Y. Wong, Automatic optic disc segmentation based on image brightness and contrast, In SPIE Medical Imaging, International Society for Optics and Photonics 76234J(2010) 1-8.

[14] U.M. Akram, S.A. Khan, Automated detection of dark and bright lesions in retinal images for early detection of diabetic retinopathy, Journal of Medical Systems 36(2012) 3151-3162.

[16] J. Lowell, A. Hunter, D. Steel, A. Basu, R. Ryder, E. Fletcher, L. Kennedy, Optic nerve head segmentation, IEEE Transactions on Medical Imaging 23-2(2004) 256-264.

[17] M. Lalonde, M. Beaulieu, L. Gagnon, Fast and robust optic disc detection using pyramidal decomposition and Hausdorff-based template matching, IEEE Transactions on Medical Imaging 20-11(2001) 1193-1200.

[25] H. Li, O. Chutatape, Boundary detection of optic disk by a modified ASM method, Pattern Recognition 36-9(2003) 2093-2104.

[26] M. Niemeijer, M.D. Abràmoff, B. Van Ginneken, Segmentation of the optic disc, macula and vascular arch in fundus photographs, IEEE Transactions on Medical Imaging 26-1(2007) 116-127.

[27] K.W. Tobin Jr, E. Chaum, V.P. Govindasamy, T.P. Karnowski, O. Sezer, Characterization of the optic disc in retinal imagery using a probabilistic approach, In Medical Imaging, International Society for Optics and Photonics 6144(2006) 1088-1097.

[32] A. Aquino, M.E. Gegundez, D. Marin, Automated optic disc detection in retinal images of patients with diabetic retinopathy and risk of macular edema, International Journal of Biological and Life Sciences 8-2(2012) 87-92.

[33] M. Foracchia, E. Grisan, A. Ruggeri, Detection of optic disc in retinal images by means of a geometrical model of vessel structure, IEEE Transactions on Medical Imaging 23-10(2004) 1189-1195.

[35] M. Niemeijer, M.D. Abràmoff, B. van Ginneken, Fast detection of the optic disc and fovea in color fundus photographs, Medical Image Analysis 13-6(2009) 859-870.

[40] L. Sukkaew, B. Uyyanonvara, S. Barman, Automatic extraction of the structure of the retinal blood vessel network of premature infants, Journal of the Medical Association of Thailand, 90-9(2007) 1780-1792.

[41] T.V. Uyen Nguyen, A. Bhuiyan, A.F. Laurence Park, K. Ramamohanarao, An effective retinal blood vessel segmentation method using multi-scale line detection, Pattern Recognition 46-3(2013) 703-715.

[42] S. Badsha, A.W. Reza, K.G. Tan, K. Dimyati, A new blood vessel extraction technique using edge enhancement and object classification, Journal of Digital Imaging, Springer United State 26-6(2013) 1107-1115.

[43] P. Bankhead, C.N. Scholfield, J.G. McGeown, T.M. Curtis, Fast retinal vessel detection and measurement using wavelets and edge location refinement, PLoS ONE 7-3(2012) 1–12(e32435).

[46] C. Duanggate, B. Uyyanonvara, S.S. Makhanov, S. Barman, T. Williamson, Parameter-free optic disc detection, Computerized Medical Imaging and Graphics 35(2011) 51-63.

Automatic Optic Disk Detection in Retinal Images Using Hybrid Vessel Phase Portrait Analysis

Nittaya Muangnak, Pakinee Aimmanee, Stanislav Makhanov

1. Introduction

One in ten of the patients with diabetes has a high risk of developing diabetic retinopathy (DR) [1]. Therefore, they are suggested to attend an annual clinical checkup. Early screening of eye diseases by ophthalmologists can help patients having diabetes to receive proper treatment at an early stage of DR. Astonishingly, according to the statistics provided by the World Health Organization (WHO), the number of people across the world with diabetes has risen very rapidly from 108 million in 1980 to 422 million in 2014 [2]. This implies the necessity of automatic screening systems to assist ophthalmologists in diagnosing early stages of ophthalmic conditions such as glaucoma, DR, or age-related macular degeneration [3] using computer-assisted diagnostics. Since eye fundus imaging is a frequent clinical procedure, the retinal fundus images are commonly used for a preliminary diagnosis and detection of suspicious cases.

The optic disk (OD) is one of the crucial points in a retina. It is important for establishing a reference frame for other regions of clinical importance inside a retinal image, such as the fovea or macula, and also to diagnose abnormalities of eye diseases. The OD usually appears in healthy retinal images as a bright, yellowish, circular, or oval object, roughly one-sixth the width of the image in diameter [4], which is partly entered by optic nerves. Any irregularity in the appearance of the OD is a sign of abnormalities or diseases such as glaucoma, DR, or hypertensive retinopathy [5].

Conventional OD detection algorithms usually rely on the assumption that the OD appears in a central position as a bright and circular object of a certain size, characterized by a certain variation of the grey level (entropy). Various researchers have attempted to identify the OD center as the largest cluster of bright pixels. The existing methods report a success rate up to one hundred percent. Similar ideas are exploited by template matching based techniques [6], [7], and [8].

A survey on the recent literature by Winder et al. [9] cited 38 papers on OD localization and segmentation. In particular, principal component analysis, active contour models (snakes), and watershed transforms and their combination were proposed in [10], [11], [12], [13]. Other models include algorithms based on intensity variation [14], Hough transform/fuzzy hybrid neural network [15], a template based approach combined with morphological operations [16], and the curvelet transform [17], [18], [19].

Pereira et al. [20] analyzed the presence of brightness on a series of blurred images and applied an Ant Colony Optimization algorithm and anisotropic diffusion. OD localization based on approximate nearest neighbor field was proposed by Ramakanth and Babu [21]. Sopharak et al. [22] applies a two-class Bayesian classifier and mathematical morphology. The Circular Hough Transform was proposed by Azuara-Blanco et al. [23]. However, Zhu et al. [24] showed that the performance of the method could be very poor even when the shape was only slightly non-circular.

One of the most efficient algorithms successfully tested against many existing methods is proposed by Lu [25]. The modification of the Circular Transform (CT) combined with evaluation of the brightness has been proven to be more efficient, more accurate, and faster than other state-of-the-art methods such as the morphological

approach proposed by Welfer et al. [26], a vessel's direction matched filter proposed by Youssif et al. [27], localization using dimensionality reduction of the search space proposed by Mahfouz and Fahmy [28], genetic algorithms proposed by Carmona et al. [29], and the local refinement active contour model by Giachetti et al. [30]. Lu's method, first, localizes the OD based on a probability map constructed from the image gradient and intensity in the horizontal and vertical directions. The circular transformation is applied next, to detect the shape of the OD. An accuracy of about 98.77% is reported (considerably higher than the competing methods).

However, a major drawback of the feature-based approaches including Lu's CT is that on poor quality images the method may generate multiple false ODs. Moreover, in these cases, physical appearance such as shape, color, brightness, or size of the actual OD becomes abnormal. An OD obscured by blood vessels or only partially visible (blur, shadows, noise) could be totally misclassified. Besides, precise OD identification based on the above-mentioned features could be sensitive to pathologies such as white/yellow lesions, exudates, or bright artifacts appearing on the retinal photographs [31].

Another important subclass of the detection algorithms is based on the convergence of the vascular network to the OD. However, only a few existing methods exploit this feature. Akita and Kuga [32] traced the parent-child relationship between blood vessels segments, tracking back to the center of the OD. Chrastek et al. [33] checked the area where vertically oriented vessels converge as a single line of infinite length. Consequently, the detection of the convergence area was reduced to the line intersection problem.

The least square polynomial curve fitting algorithm and multilevel thresholding technique were applied by Kavitha and Devi [34] to localize the OD by detecting the strongest convergence point of blood vessels. A geometrical parametric model was proposed by Foracchia et al. [35] using the parabolic approximation of the vascular network to describe the general direction of retinal vessels at any given position in the image. The vessel directions were parameterized and the simulated optimization was used to obtain the coordinates of the center of the OD.

Niemeijer et al. [36] applied a k-Nearest Neighbor regression and a circular template on all vessel pixels to locate the OD. Proposed by Dehghani et al. [37], the OD was identified by finding the region having the highest density of vessels, corners, and bifurcation points using Harris corner detection. This algorithm was effective under invariance of rotation of retinal images, whereas the presence of pathological regions needed to be distinguished, and the desired OD contour required high variance contrast between OD and the surrounding background.

Welfer et al. [26] and Zhang and Zhao [38] used the assumption that the major vessels line up horizontally. The major drawback of these approaches is that they are not rotationally invariant. Vascular networks and intensity information were combined to examine the entropy of vascular directions in Mendonca et al. [39]. The distribution of vessel orientations around an image point is quantified using the entropy of vascular directions. The OD localization is done by searching for the high intensity image area that has maximal values of entropy. The active contour (snake) was employed by Semashko et al. [40]. The positions of the vessels were used to correct the pressure force of the active contour to improve the convergence of the snake to the OD center.

Rangayyan et al. [41] used Gabor Filters to detect vessels to produce the orientation field. The resulting vector field was analyzed by the Phase Portrait Analysis (PPA) to detect the points of convergence. The method reported an accuracy up to 100% on the DRIVE database [42], however, the method failed when applied to poor quality images from STARE [43] (69.1 %). The main reason for that is that the vessels extracted from the poor quality images usually create an inappropriate vector field. Consequently, the PPA generates multiple convergence points

and a false OD.

In this paper we show that a proper vector field can be generated using a certain set of features at the bifurcation points. These features (rather than the direction of blood vessels) combined with some additional vectors allow us to process poor quality images. For instance, the accuracy of the PPA on STARE has been increased to 99%.

Another outstanding vessel convergence technique was introduced by Hoover and Goldbaum [4]. The method, called *Fuzzy Convergence (FC)*, created a fuzzy segment of which an area was provided by a voting scheme for corresponding pixels of each segmented vessel. An image map, representing the strong points of the convergence, was calculated by summation of votes. The map was then smoothed and the strongest convergence points are detected by thresholding. The fuzzy convergence technique was combined with a feature-based approach which employs illumination equalization to minimize the large intensity variation at different scales. Method verification on the STARE database showed acceptable performance overall (89%), and full success on the healthy retina images (100%). Nevertheless, the hierarchical structure of the retinal vessels and their importance were not considered. The retinal vessel network consists of both skeletonized primary and secondary attributes to the optic nerve head. The main vessels converge to the OD, whereas the secondary vessels are positioned randomly.

In this paper we use the fact that the geometry of the vessels converging at bifurcations indicate the direction to the OD. In order to find these directions, the smallest branching angle is evaluated at each bifurcation. We assume that the "main" vessel directed to the OD is opposite to the smallest branching angle. This assumption is not always correct when we consider pathological cases comprising individual fuzzy and distorted blood vessels. However, for the majority of the images (even with poor quality) the smallest bifurcation angle points in the correct direction. Moreover, in order to define the main vessel we consider not only the branching angle, but selected features as well i.e. thickness, tortuosity, and intensity. In addition, other connected vessels are considered.

In order to improve the quality of the resulting vector field, sole vessels are also taken into account, based on their importance. Besides, the bifurcation vectors have been supplemented by the so-called Mahfouz's vectors [28], based on the observation that the vessels are positioned predominately along the vertical direction.

Our new technique is the above representative vectors, interpolation of these vectors throughout the entire image, and analyzing the resulting vector field by phase portrait analysis (VVPPA). The VVPPA approach is combined with the Vessel Transform (VT) [44], based on the clustering the vessels into the binary trees and using a decision rule-based method. The combination of VVPPA and VT is called the Hybrid Method(HM). The HM is integrated into the scale space analysis proposed in [45] . The new algorithm has been tested on fair and poor quality retinal images from two databases (172 images) against the fuzzy convergence method [4], a recent modification of the Circular Transform [25], and the VT [44] applied without the hybridization with VVPPA. Furthermore, the space scale boundary detection [45] was tested with and without the VVPPA and the HM. The numerical experiments demonstrate that the proposed algorithms outperform the baseline methods in terms of the precise localization of the OD and the accuracy of segmentation in the framework of the space scale scheme.

The paper is organized as follows. Section 2 describes two novel approaches for OD localization. Section 3 describes the proposed method of OD segmentation. Section 4 describes the data collections and setup of our experiments. Section 5 shows results. Section 6 provides a discussion of the results and limitations of the approach. The last section concludes the work.

2. Our Proposed OD localization Approaches

In this section, we present *Vessel Vector based Phase Portrait Analysis Approach (VVPPA)* and *Hybrid Method (HM) comprising VVPPA and VT*.

2.1 Vessel Vector based Phase Portrait Analysis Approach (VVPPA)

Five types of vectors are defined in the framework of VVPPA namely

1) The shifted leading bifurcation vectors (SLBV)
2) The sole vessel vectors (SVV)
3) The Mahfouz vectors (MV)
4) The bouncing vectors (BV)
5) The interpolated vectors

The SLBVs are constructed by considering *bifurcation* associated with three vessel segments. A circle centered at a junction with radius *r* is drawn and the intersection points of this circle with the vessel segments are marked. Normalized vectors from the junction to the intersection *are the bifurcation vectors* (Figure 1). Next, the leading vectors are classified from these bifurcation vectors using the opposite angle, tortuosity, thickness, and contrast. The opposite angle of a vector is an angle between the other two vectors originated from the same bifurcation point. Tortuosity is the ratio of the distance to the displacement of two end points of the vessel segment. Thickness is the average width of the vessel segment considered only from the bifurcation point to the intersection point. Contrast is the difference of the cumulative intensity between the vessel segments and their surrounding background from the bifurcation point to the intersection point. The angle, tortuosity, thickness, and contrast are normalized. The classification is based on the SVM method [46] applied with the training and testing sets. The rules obtained from the training set are applied to the testing collection. Once the leading vector is obtained, we shift it along its direction to the end of the corresponding vessel. This vector is the *SLBV* in Figure 1. The *SLBV* is used rather than the leading vector because it is closer to the OD. Therefore, it will produce a better vector field.

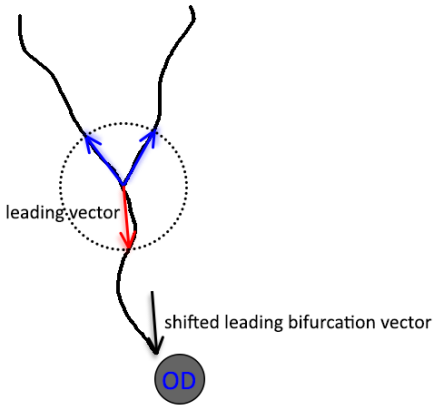

Figure 1 The illustration of a shifted leading bifurcation vector

The SVV are often the main vessels. Therefore, they contribute useful information about the OD location. To generate the SVV, we selected the sole vessels which are not too short, not too thin, and not too faint using a threshold selection technique. For each SV, we randomly pick a direction and normalize the resulting vector. The

directions of the SVVs are to be corrected later in the VVPPA algorithm.

The probabilistic OD approximation proposed by Mahfouz and Fahmy [28] is also taken into consideration. The Mahfouz's approach is based on the simple observation that the central retinal artery and vein emerge from the OD mainly in the vertical direction and then progressively branch into main horizontal vessels. From the vascular structure of the retina, a vertical bar with an image height and a proper width would always be dominated by vertical edges (vertical vessels) when centered at the OD. Thus, the *x-location* that yields the greatest difference between vertical edge and horizontal edge is the vertical location of the OD. Once the vertical location is obtained, the *y-location* is determined by considering a square window with length equal to the average diameter of the OD, using this horizontal location to find the location that has the highest number of bright pixels. Four unit vectors derived from Mahfouz's approach are created at the top and bottom as well as at the right and left edge of the retina (Figure 2).

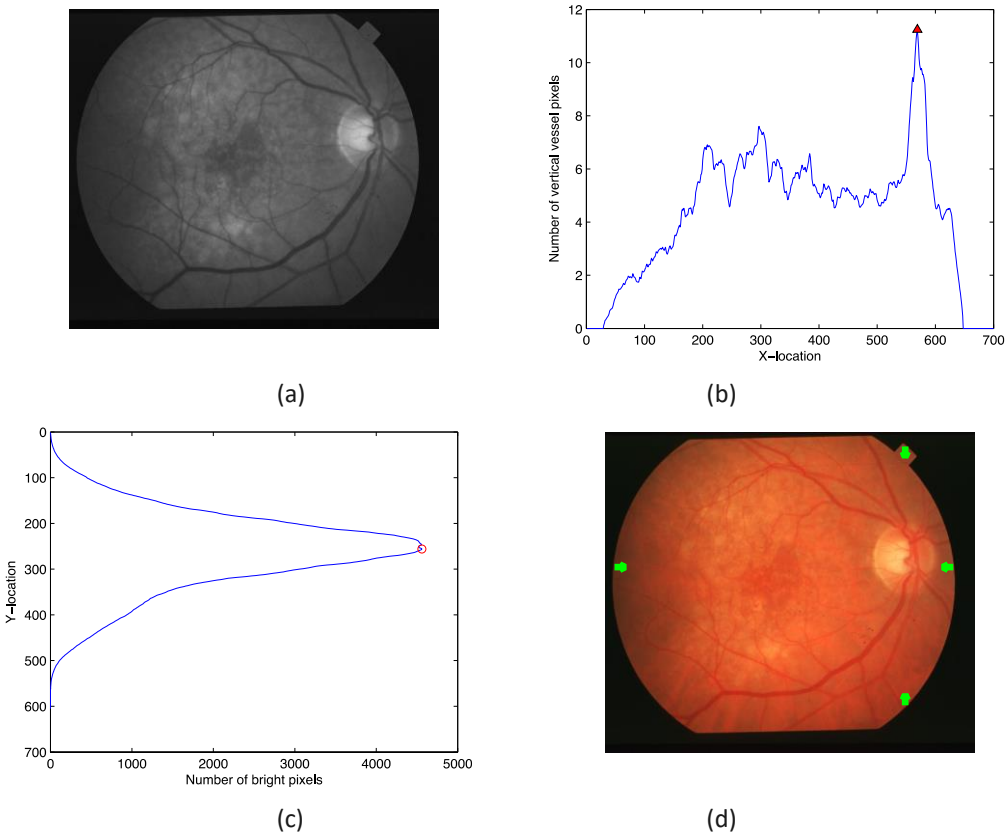

Figure 2 Mahfouz vectors (a) original image (b) the greatest difference of the number of pixels in the vertical edge and horizontal edge. (c) y-location vs. the maximum number of bright pixels in a reference square at the x-location (d) the Mahfouz vectors.

The Mahfouz's approach is experimentally proven to be fairly accurate for up to 92.6% [28]. It usually works

well when the vessel structure is complete and the OD is clear. We thus employed vectors derived from the Mahfouz's approach to be a part of the proposed algorithm. However, when the quality of the images is poor, the Mahfouz's approach may not yield good accuracy. However, in many cases the MV contribute to the proposed algorithm.

The BVs are created with the purpose to improve the convergence area of PPA. A bouncing vector of a vector V is a unit vector starting at the edge of retinal image and pointing opposite to V. In this work, the bouncing vectors are derived from SLBV, SVV, and MV.

The last type involved with the proposed algorithm is the *interpolated vector* constructed at every grid point of the retinal image using triangulation of the image and linear interpolation. The vector flow is assumed to change linearly in the neighborhood of the critical point as follows, $v = Ap$, where $v \equiv (x, y)$ the Cartesian coordinate, and *A* is the corresponding matrix. The matrix is approximated by the least square method applied to *v* in the moving window centered at *p*. The flow patterns characterized by the eigenvalues of matrix *A* are shown in Table 1, where λ_1, λ_2 are the eigenvalues, $R_i = Re\ \lambda_i$, $I_i = Im\ \lambda_i$, and *i* = 1, 2. Table 1 shows the patterns used in this study (see [47] for the entire collection). The proposed vector field classifier employs a continuous formulation given by

$$C(\lambda_1, \lambda_2) = \begin{cases} \dfrac{\min(|\lambda_1|, |\lambda_2|)}{\max(|\lambda_1|, |\lambda_2|)} \dfrac{sign(\lambda_1 \lambda_2) + 1}{2}, & if\ \lambda_1 > \delta, \lambda_2 > \delta \\ 0, & otherwise \end{cases}$$

where δ is a threshold to exclude ill conditioned matrices characterized by small eigenvalues. The term $\frac{\min(|\lambda_1|,|\lambda_2|)}{\max(|\lambda_1|,|\lambda_2|)}$ includes converging/diverging configurations, i.e. attracting and repelling stars, as well as strong attracting and repelling nodes, such that $C(\lambda_1, \lambda_2) \approx 1$ (see Table 1). We shall call these converging configurations [47].

Table 1 Phase portrait analysis of the 2D vector flow

Pattern	Eigenvalues		Illustration
Saddle Point	$R_1 > 0, R_2 < 0$	$I_1 = I_2 = 0$	
Repelling Node	$R_1 \neq R_2 > 0$	$I_1 = I_2 = 0$	
Attracting Node	$R_1 \neq R_2 < 0$	$I_1 = I_2 = 0$	
Repelling Star	$R_1 = R_2 > 0$	$I_1 = I_2 = 0$	
Attracting Star	$R_1 = R_2 < 0$	$I_1 = I_2 = 0$	
Saddle node (edge)	$R_1 = 0, R_2 \neq 0$	$I_1 = I_2 = 0$	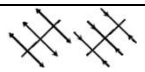

Therefore, the PPA algorithm returns the location of the converging configurations, one of which points to the OD. The entire VVPPA algorithm is presented below.

Input:
SLBV: Shifted leading bifurcation vectors
MV: Mahfouz vectors
BV: Bouncing vectors

SVV: Sole vessel vectors {svv_1, svv_2, …, svv_k}
Output: *centroid of the convergence region*

VVPPA Algorithm:
V = {SLBV, MV, BV}
IV=Make_InterpolationVectors(V)
#Determine the convergence region from PPA scores
CovReg = Find_HighPPAScore_LargestRegion(IV)
c = Find_Centroid(CovReg)
for i = 1:k
#Validate the direction of the sole vectors
if Is_Pointing_outward(svv_i, c) is true
$svv_i = -svv_i$
endif
#Correct the location of convergence region
$V = V \cup \{svv_i\}$
IV= Make_InterpolationVectors(V)
CovReg = Find_HighPPAScore_LargestRegion(IV)
c = Find_Centroid(CovReg)
endfor

In this algorithm, *Make_InterpolationVectors(V)* takes the collection of the input vectors V to generate the interpolated vectors, IV, at all grid points in the retina image. *Find_HighPPAScore_Region(IV)* finds and returns the region (CovReg) high PPA scores obtained using the input collection IV. There can be many regions characterized by high PPA scores. Therefore, we select the final region using the maximum likelihood estimation based on: the mean thickness of segmented vessels, the contrast of segmented vessels compared to surrounding background, the density of segmented vessels, and the original PPA scores. *Find_Centroid(CovReg)* returns the centroid of the convergence region *CovReg*. *Is_Pointing_outward(v, c)* returns true if *v's* direction is toward cs, otherwise false. Figure 3 illustrates the above VVPPA techniques.

2.2. Hybrid Method

An enhanced version of VVPPA is called the Hybrid Method (HM). The HM combines the vessel transform (VT) [44] and VVPPA. The VT approximates the location of the OD by finding a centroid of a collection of points, of which the total sum of the distances from each point in this collection to all vessel clusters is minimal. This HM aims to carry out the best accuracy of the VT and VVPPA approaches. To localize OD, the HM creates a decision model to select an appropriate approach (VT or VVPPA). The decision is based the number of bifurcation vectors, the number of sole vessel vectors, and the PPA score. The HM pseudo-code is given below

Input:

C = A collection of images of size N
I = A collection of testing image of size P
T = Input a training set of images of size N_t, $N_t < N$
F(T) = {F_1(T), F_2(T) …, F_M(T)} where F_i(T) is the i^{th} feature vector extracted from T
ANS(T) = a binary answer set vector (0 for VT and 1 for VVPPA) of T of size N_t

Output:

algV = a binary vector containing answers

Hybrid Algorithm:

% generate the decision model

DModel= Calculate_Decision_Model(F(T), ANS(T))
% Determine the answer for the testing image
FI = {F_1(I), F_2(I) …, F_M(I)}
algV = Select_Algorithm(DModel, FI)

The *Calculate_Decision_Model(F(T), ANS(T))* generates the decision using the feature matrix *F(T)* and the training set *ANS(T)*. *Select_Algorithm(DModel, FI)* returns the algorithm that should be used for testing the collection using the *DModel* obtained from the *Calculate_Decision_Model(F(T), ANS(T)). FI* is the feature matrix associated with the testing set.

As the HM builds the model from the best results from both approaches, its performance is usually better than both VT and VVPPA. The HM reduces the computational time to approximately half relative to each individual approach.

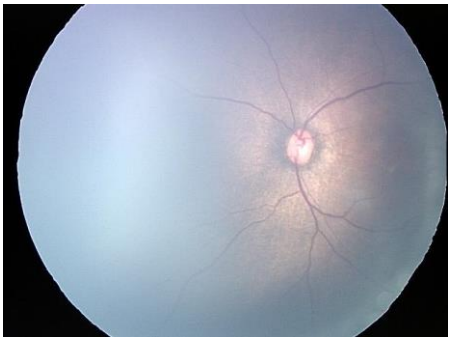

(a) Original image

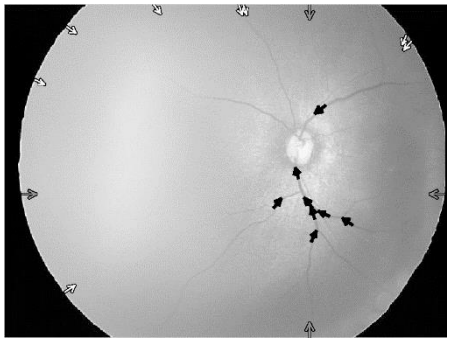

(b) SLBV (black), MV (gray), and BV (white)

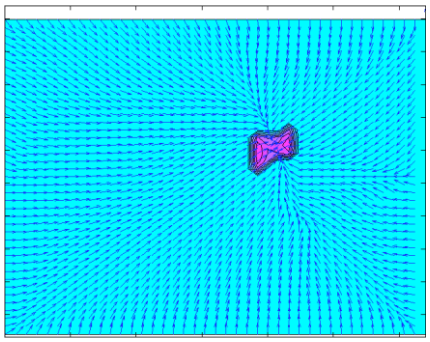

(c) IVs and the initial CovReg

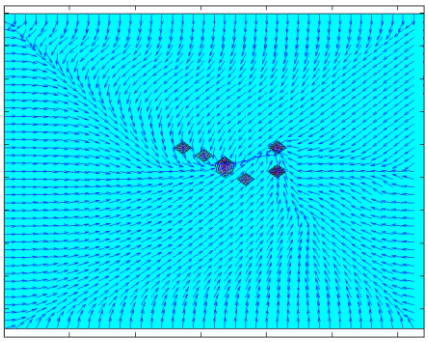

(d) IVs and CovReg after including the 1st sole vector

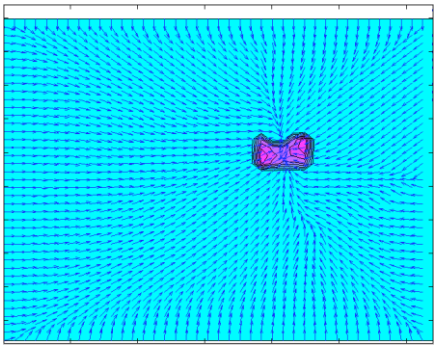

(e) IVs , CovReg after including the 2nd sole vector

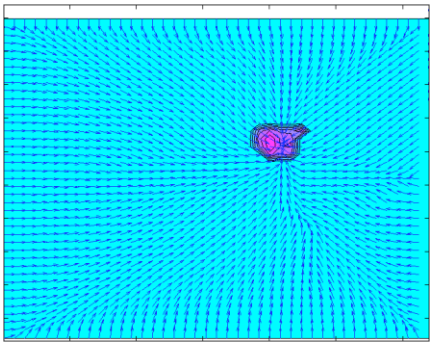

(f) IV, CovReg after including the 3rd sole vector

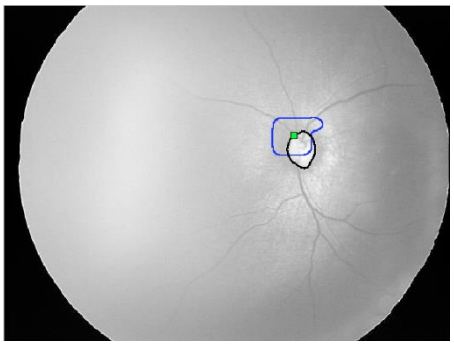

(g) Centroid (green rectangle) of CovReg boundary (blue line) and the ground truth boundary (black line)

Figure 3 Illustration of the VVPPA algorithm

3. Scale Space Algorithm with VVPPA/HM for OD Segmentation

The Scale Space(SS) theory was originally proposed by Witkin [48] to create a multi-scale representation of signals in 1-D. Lindeberg [49] applied the SS to image segmentation. The SS theory was applied by Duanggate et al. [45] for OD segmentation in the retinal images. In their work, a series of images resulting from applying the Gaussian smoothing were constructed. The blobs (or closed contours) that exist over smoothen images were linked and represented as a scale-space blob tree. The merging processes are applied to merge together the blobs that meet the criteria of blob adjacency and also stability, measured by relevant attributes. The OD blob is selected from these candidate blobs based on four features of OD: size, entropy, intensity, and compactness. This OD blob represents the OD. We integrate the SS scheme with VVPPA and with HM. In the framework of the SSVVPPA approach, the SS theory is modified by employing the PPA score along with the original features used in Duanggate's work. For the SSHM approach, the SS theory is combined with either the vessel transform (VT) [44] or VVPPA. The choice of method to be combined with SSC depends on the answer returned by the HM. If the HM returns VT, the vessel transform score is considered together with the original features in the OD selection process of SS.

As the boundary of the OD blobs obtained from SS can be wavy, which does not reflect the round shape of the OD, we readjust the boundary using a circle. Such a circle is centered at the centroid of the OD blob and has a radius equal to one half of the average diameter of the OD in the collection. We call these three SS family schemes: SS, SS combined with VVPPA, and SS combined with HM, with adjusted circular boundary *SSC, SSVVPPAC*, and *SSHMC,* respectively.

4. Numerical Experiments

We consider a standard database STructured Analysis of the REtina (STARE) [43]. The fundus photographs from STARE were captured by a TopCon TRV-50 fundus camera with 35° field of view. Each image was digitized to create a 605 x 700 pixels at 24 bits per pixel. Another collection is a dataset originally collected to detect the signs of retinopathy of prematurity (ROP) by Dr. Sarah Barman at Kingston University of UK. All digital images from ROP were taken from patients with non-dilated pupils using a KOWA-7 non-mydriatic retinal camera with a 45° field of view. The images were stored in JPEG format, 640 x 480 pixels at 24 bits per pixel. We classify images into two categories. The bright, round, and clear ODs are classified visually as "fair". The rest is considered "poor".

There are 91 images for the ROP collection with an average OD diameter of 47.88 pixels. Sixty images are

classified as fair and 31 as poor. STARE includes 81 images with an average OD diameter of 103.88. There are 31 images of fair quality and 50 images of poor quality. Examples of fair and poor retinal fundus images are displayed in Figure 4.

To evaluate the proposed methods, hand-drawn ground truth (GT) images were obtained from human experts. To minimize the human expert bias, the GTs were obtained from three ophthalmologists from Thammasat University Hospital. Each ophthalmologist was asked to hand-draw the OD contours on each retina image from two collections three times. The inter-observer between different ophthalmologists and intra-observer variability within the same ophthalmologist were determined by finding the ratio of the area that at least two out of three GT images are intersected to the area that are the union of all GTs. The inter-observer variability is 0.86 and 0.91 for the ROP and STARE collections, respectively. The intra-observer variability, defined as the score from the three GT contours obtained by the same expert, are 0.91 and 0.93 on average, for the ROP and STARE collections, respectively.

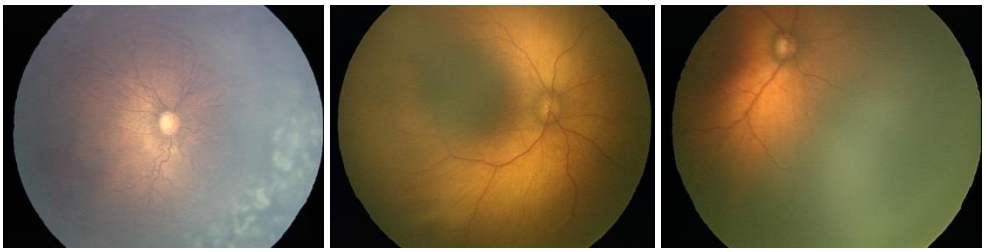

(a) Fair images

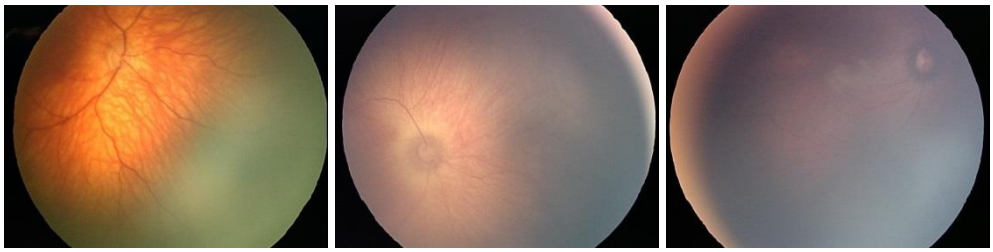

(b) Poor images

Figure 4 Examples of “fair” and “poor” images

Since the two collections of the test images have been obtained by different devices with different illumination conditions, they require different decision models for leading vector classifications.

In order to classify the leading vectors, we employ the SVM classifier with the Gaussian kernel [50]**.** We trained the method using the standard 70-30% ratio between the training and the testing data. An example of the decision models for leading vector classification is shown in Figure 5 where red and blue markers represent the feature values of the leading and non-leading vectors, respectively. The X, Y, Z-axes represent the normalized values of the three features: the opposite angle, the tortuosity, and the intensity, respectively. The black line indicates the decision boundary. The accuracy of the SVM model on the testing set is 96.61% and 94.11% for ROP and STARE, respectively.

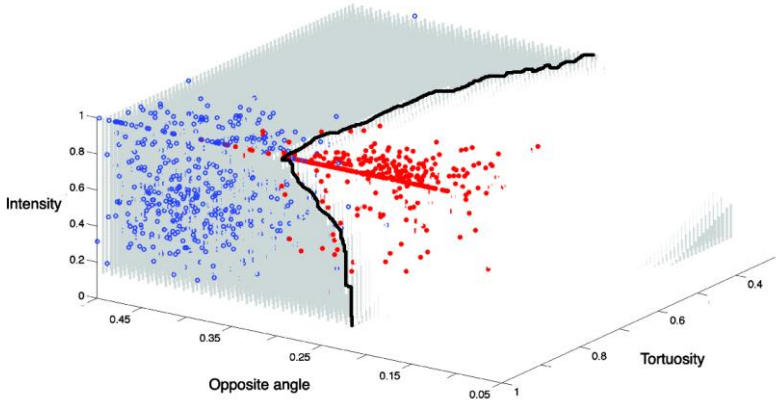

Figure 5 The SVM decision model: red diamond – leading vectors and blue circle – the non-leading vectors

In order to classify the candidate blobs produced by the SS procedure into the OD and nonOD groups, we use the automatic decision tree generator available from the Waikato Environment for Knowledge Analysis [40]. The 70/30 ratio was used for the training and testing. The corresponding decision tree requires the following features: the PPA score, size, compactness, entropy, and intensity denoted by *p, s, c, e,* and *i*, respectively. The following decision trees shown in Figure 6 are used for classification of OD and nonOD. The constructed decision trees reveal that all features except intensity are important in detecting the OD.

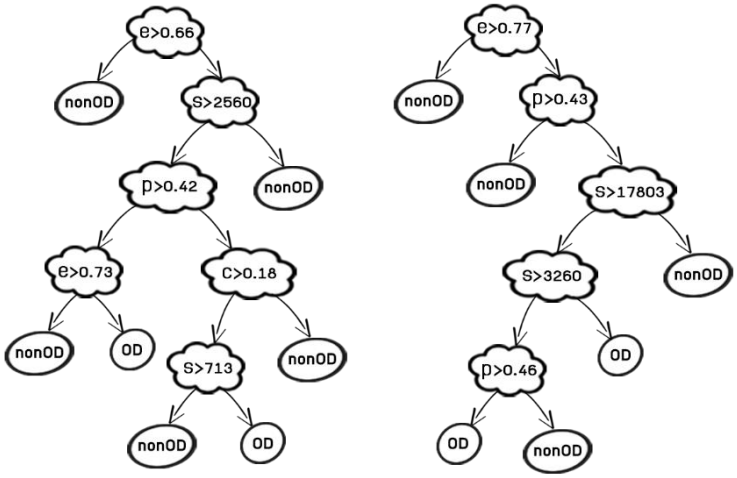

Figure 6 SSVVPPAC decision trees (left) the ROP collection, (right) the STARE collection

As far as the SSHMC is concerned, the features derived from VVPPA were considered mainly as the basis model rather than those of VT due to the fact that features obtained from VT require longer computational time [44]. The features include the number of SLBV, the number of SSV, and the PPA score. The decision model applied to both ROP and STARE is presented in Figure 7.

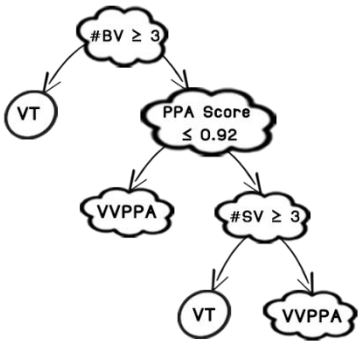

Figure 7 The decision tree of the HM for OD localization

5. Results

In this section, we test VVPPA and the HM against the Fuzzy Convergence (FC) method [4], a recent modification of the Circular Transform proposed by Lu (CTL) in [25] and our previous vessel transform method (VT) [44]. For the OD segmentation, we compare the results of SSVVPPAC and SSHMC against the SSC, CTL, and SSVTC [41].

5.1 Performance of the VVPPA and HM in Locating the OD

We test the VVPPA and HM against CTL method [25], Fuzzy Convergence method [4], and the vessel transform method (VT) [44]. Figure 8 shows introductory examples of the OD location obtained by the VVPPA and HM vs. the three baseline approaches. VVPPA and HM generally perform better. The accuracy of OD localization is evaluated as follows. If the OD location is contained entirely inside the circle centered at the GT's centroid (the radius equals to the average GT radius of the collection), we considered this a correct result. The ratio of the correct cases to the total number of images yields the average accuracy. CTL is considered successful if the centroid of the CTL contour is located inside the ground truth contour.

The numerical accuracies of five competing OD localization methods are shown in Table 2.

Table 2 Accuracy of the OD localization using FC, CTL, VT, VVPPA, and Hybrid, percent

Collections	ROP		STARE		Overall average	Overall average for fair	Overall average for poor
Image Quality/Method	Fair	Poor	Fair	Poor			
FC	N/A	N/A	90.32	88.00	N/A	N/A	N/A
CTL	88.33	64.52	100.00	98.00	87.71	94.16	81.26
VT	95.00	96.77	96.77	94.00	95.64	95.88	95.38
VVPPA	**100.00**	83.87	**100.00**	96.00	94.97	**100**	89.93
HM	**100.00**	**96.77**	**100.00**	**98.00**	**98.69**	**100**	**97.38**

The proposed approach outperforms CTL on both test collections and shows a better success rate against CTL by 7.26 and 10.98 percent, using VVPPA and HM, respectively. Even though VVPPA shows a reduction of accuracy against VT by 0.67 percent, the HM works better than VT with an absolute improvement of 3.05 percent. For all image collection differentiated by image quality, the absolute improvements of VVPPA and HM are noticeably better than CTL by 8.67 and 16.12 percent, respectively for the poor sets, and by 5.84 percent for the fair sets. When

VVPPA and HM are compared to VT, they show an improvement in the fair sets by 4.12 percent. While the VVPPA success rate is lower than VT by 5.45 percent, the HM outperforms VT by 2.00 percent for the poor sets. Finally, among the tested methods, the HM yields the best performance in all categories.

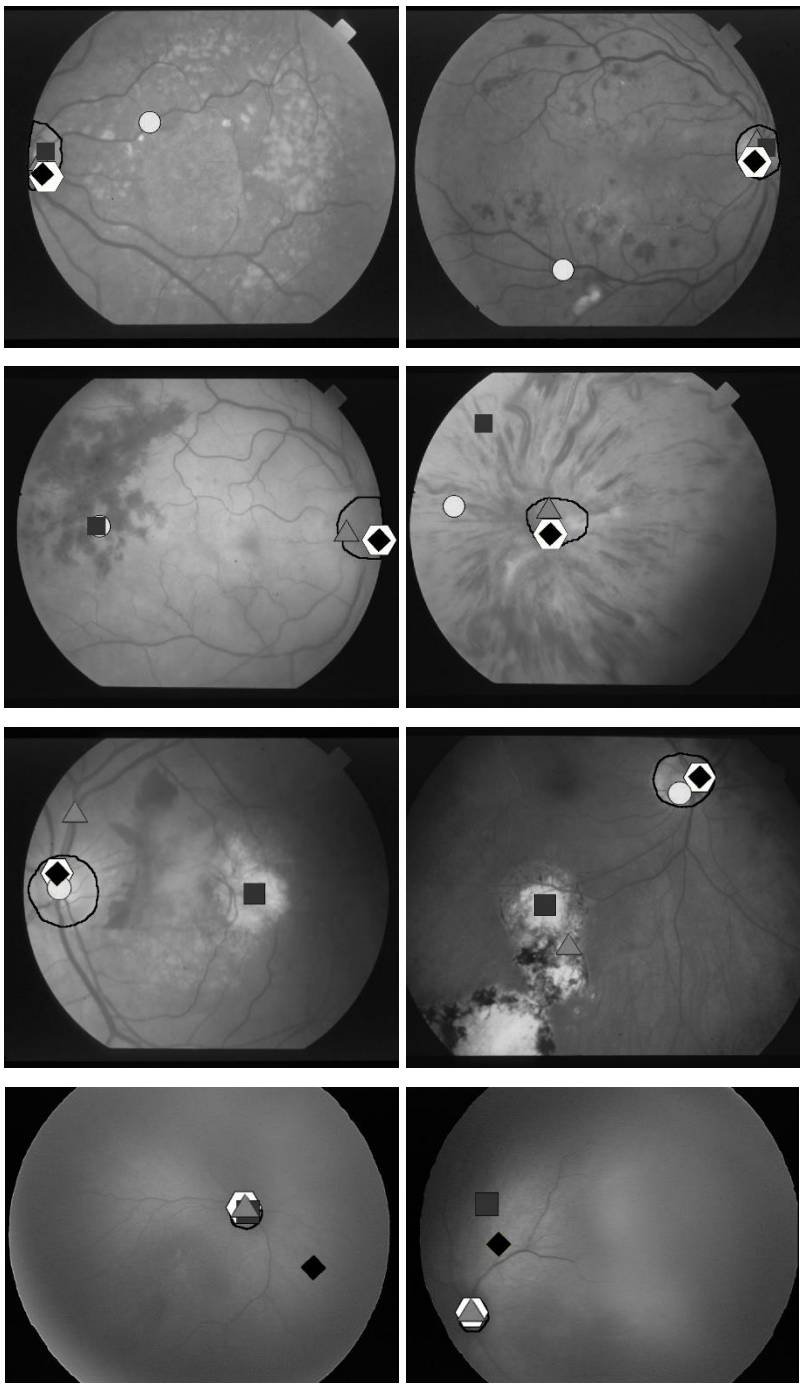

Figure 8 Examples of the OD location results: Ground truth –black solid line, FC – light gray circle, CTL– dark gray square, VT – gray triangle, VVPPA – black diamond, and HM –white hexagon.

5.2 Performance of SSVVPPAC and SSHMC

In this section, we present the results of the OD segmentation based on the SS algorithm with information from our OD localization approaches together with circular edge adjustments [45]. SSVVPPAC and SSHMC are compared with three OD segmentation method: CTL, SSC, and SSVTC. Figure 9 shows the qualitative results of OD segmentation obtained by using different approaches. Table 3 shows the corresponding sensitivity and positive predictive value (PPV). The bold font presents the best result in a particular category. The two standard schemes reveal the correctness and reflect the completeness of the attained solution. The sensitivity is defined to be the ratio of the number of pixels detected correctly as the OD to the total number of pixels detected as the OD. The PPV is the ratio of the number of pixels detected correctly as the OD to the total number of pixels of the OD from the ground truth.

Table 3 The Accuracy of the OD segmentation using CTL, SSC SSVTC, SSVVPPAC, and SSHMC, percent

Evaluation	Methods	ROP		STARE		Average on all collections	Average for fair sets	Average for poor sets
		Fair	Poor	Fair	Poor			
Average Sensitivity	CTL	74.29	61.28	72.59	41.23	62.35	73.44	51.26
	SSC	87.74	51.38	65.62	49.86	63.65	76.68	50.26
	SSVTC	**89.60**	**80.07**	**76.14**	59.97	76.45	**82.87**	70.02
	SSVVPPAC	**89.60**	72.72	75.30	59.94	74.39	82.45	66.33
	SSHMC	**89.60**	**80.07**	75.30	**61.26**	**76.56**	82.45	**70.67**
Average PPV	CTL	66.42	46.39	**84.66**	69.89	66.84	75.54	58.14
	SSC	80.56	49.84	62.19	57.54	62.53	71.38	53.69
	SSVTC	**81.91**	**72.53**	70.86	70.27	**73.89**	**76.39**	71.40
	SSVVPPAC	**81.91**	65.17	70.05	69.10	71.56	75.98	67.14
	SSHMC	**81.91**	**72.53**	70.05	**71.08**	**73.89**	75.98	**71.81**

The proposed method has been compared with the baseline methods in Table 3 in terms of the average sensitivity of all collections. The SSHMC returns outstanding absolute improvement over CTL, SSC, and SSVTC by 14.21, 12.91, and 0.11 percent, respectively. For the average PPV, SSHMC shows an absolute improvement against CTL and SSC, respectively, by 7.05 and 11.36 percent, and equivalent performance relative to SSVTC.

Furthermore, the proposed approach performs better for the fair quality sets in all collections, for both sensitivity and the PPV. The SSVVPPAC and SSHMC show the largest absolute improvement (sensitivity and PPV) for the fair set for the both collections by 9.01 and 0.44 percent against CTL, 5.77 and 4.61 percent against SSC, and only slightly degradation by 0.42 and 0.41 percent against SSVTC, respectively.

For the poor sets of both collections, SSHMC shows significant improvement in sensitivity of 19.41, 20.05, and 0.64 percent when compared against CTL, SSC, and SSVTC, respectively. In comparison, SSHMC yields a noticeably higher average PPV than CTL as its absolute improvement of SSHMC against CTL is 13.67 percent. In comparison with SSC, the maximum average PPV of SSHMC has been improved considerably by 18.12 percent.

Generally the proposed approach outperforms SSC and CTL regardless of the quality of the images and for each collection of data. In particular, when the image quality is poor, the proposed approaches outperform the other two methods substantially.

It should be noted that in [45], the SS method was found to be superior with regard to OD segmentations based on the morphological operations [22] and the Circular Hough Transform [51]. Moreover, in [25], Lu claims to outperform a genetic algorithm and direct search approach [29], a geometrical model of vessel structure using two

parabolas [35], a feature and vessel based approach [52], and a morphologic two-stage approach [53]. Therefore, the proposed approach outperforms the above-mentioned methods as well.

The SSHMC is a combination of VVPPA and VT designed to produce better accuracy. The average improvement of SSVVPPAC and SSHMC on both collections against CTL method is, respectively, 12.04 and 14.21 percent, for the sensitivity, and 4.72 and 7.05 percent, for the PPV. In turn, the improvement produced by SSVVPPAC and SSHMC vs. SSC is respectively, 10.74 and 12.91 percent, for the sensitivity, and 9.03 and 11.36 percent, for the PPV.

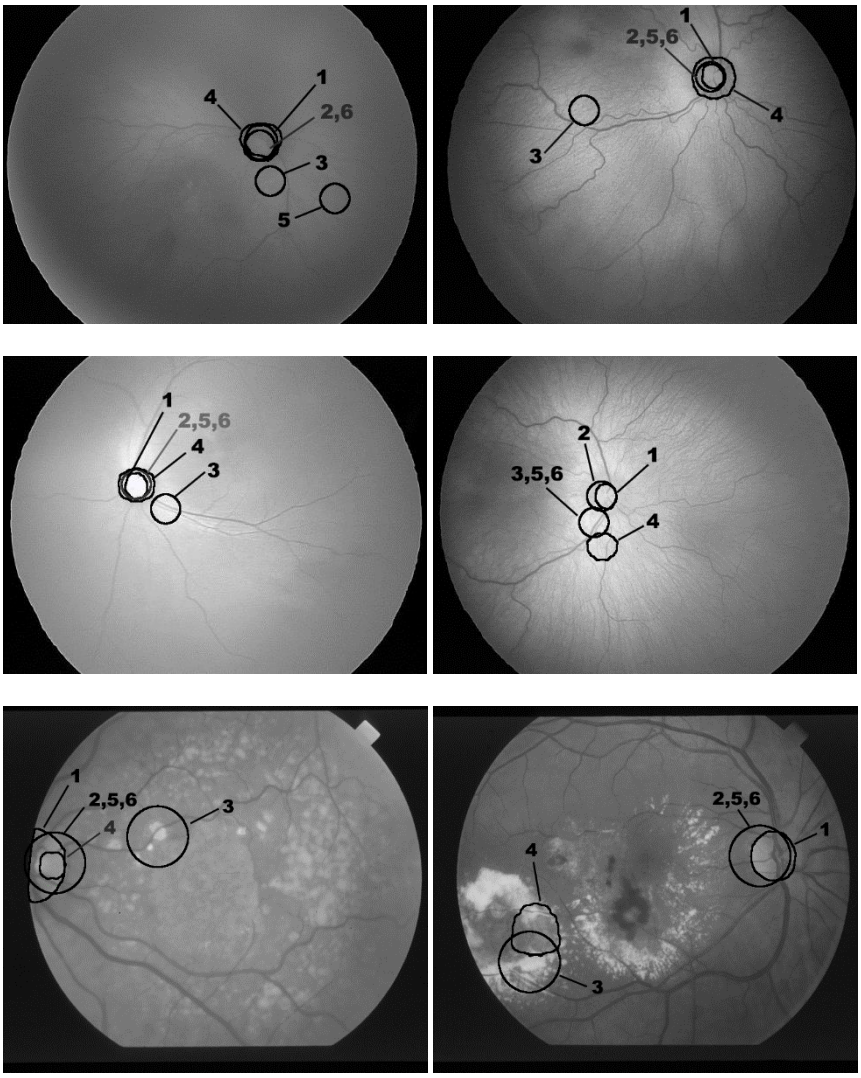

Figure 9 Examples of the OD regions: 1-GT, 2-SSVTC, 3-SSC, 4-CTL, 5- SSVVPPAC, 6-SSHMC

5.3 Computational Time

Although the CTL method is claimed to be the fastest, its performance strongly depends on the threshold of the gray level (to select possible candidates for the center of the OD) and the number of radial segments used to verify the circularity of the object boundary. Lu also claims that the OD center always lies within the first 20% brightest pixels within the probability map of the OD. However, there are a number of poor quality images for which this is not correct. The increase of the above thresholds increases the computational time nonlinearly. For instance,

changing the percentage of the brightest pixel threshold from 20 to 60% doubles the computational time, whereas changing the angular step from 6° to 2° increases the computational time of the CTL method by a factor of 10. Our method, programmed in MATLAB, requires on average of about 3 minutes processing on a standard database image 600x750 on a Dell computer with 3.30 GHz Intel Core i3 Processor with 4GB of random access memory. Table 4 shows the average computational time of SSVVPPAC and SSHMC against CTL and SSVTC.

Table 4 Computational time per image (≈400x400): CTL vs. the proposed method

Percentage of test pixels (%)	No. of radial line segments	Average time: CTL (min)	Average Time (min)		
			SSVTC	SSVVPPAC	SSHMC
20	40	1.57	4.85	2.55	2.85
20	180	6.63			
60	40	4.29			
60	180	18.84			

Furthermore, SSVVPPAC and HM are twice as fast as the VT approach, which is about 2 minutes per image.

5.4 Discussion

In this section, we present typical cases when the proposed method fails to work. For OD detection, the incorrect locations occurred by VVPPA are due to not enough information from the vessels and the presence of vessel-like reflection. As VVPPA and HM require sufficient numbers of vessel branches in order to make a strong PPA convergence, thus when there are only one or two initial vectors, it can lead to the incorrect location of the OD. Another cause is due to a false vessel which may result from shadow, lesions and/or uneven illumination in the image. These types of components in the image can produce incorrect vectors resulting false location of OD. Figure 10 shows a case of insufficient information from vessels (the left image) and a case that the shadows ,and the uneven illumination in the image cause false vessel input for the vessel segmentation algorithm (the right image).

As HM uses either VT or VVPPA, the performance of HM also depends on VT and VVPPA. Because VT relies primarily on vessels as well, then the previously mention reasons can cause VT to fail to detect the OD. When such a case occurs, the user is suggested to use other approaches which depend on the OD features instead.

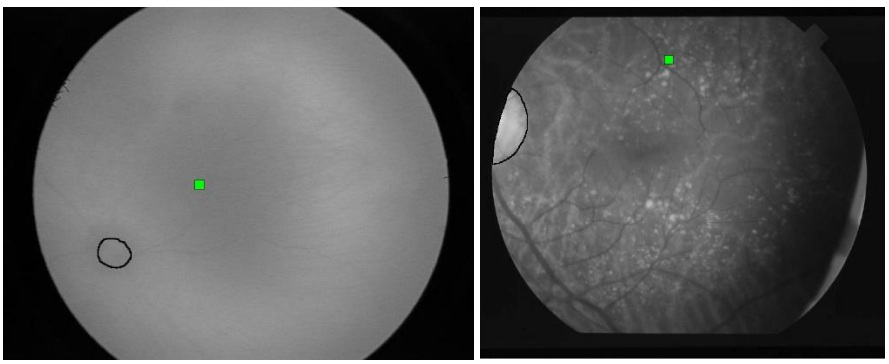

Figure 10 Examples of cases that our proposed approaches fail due to insufficient vessel information. Green rectangle shows the OD location obtained by VVPPA.

For the OD segmentation, the error comes from two major sources. Both sources are features that are used in the OD selection process. First is the incorrect information obtained from the OD features: size, entropy, intensity, and compactness. The incorrect information are due to non-OD components such as lesion, hemorrhage, or shadows that share similar feature as the OD. Second is the incorrect information from OD location obtained from our proposed approaches. The causes of this incorrect location are described earlier. Figure 11 shows examples of images of which SSVVPPAC fail to locate OD.

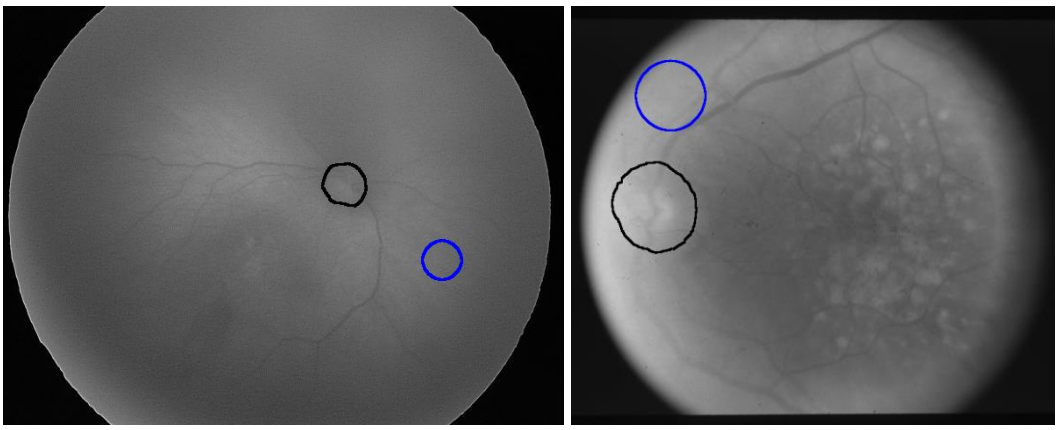

Figure 11 Examples of cases that SSVVPPAC fails completely to segment the OD (black- ground truth, blue- SSVVPPAC)

As the SSHMC uses the advantages of both SSVTC and SSVVPPAC, it carries the disadvantages of SSVTC and SSVVPPAC as well.

6. Conclusions

Novel approaches, based on a combination of VVPPA and HM, are proposed. VVPPA localizes the OD by detecting vessels pointing out to the OD in bifurcation points and analyzing the resulting vector field by PPA. The vessels at the bifurcation points are classified by SVM using a set of appropriate features. The leading vectors have been complemented by the Mahfouz approach and synthesized bouncing vectors created to ensure the convergence to the OD.

The Hybrid Method is based on a decision tree, utilizing a certain set of features which determines when VT and VVPPA should be used. Furthermore, to obtain the OD boundary, VVPPA and Hybrid methods are integrated into a segmentation algorithm based on SS techniques with a circular edge adjustment. The integration generates new SSVVPPAC and SSHMC. The PPA scores obtained from VVPPA are used as the additional features in the based scale space approach [45]. The Hybrid approach incorporates either VT or VVPPA features selected by the corresponding decision tree.

The numerical experiments on OD localization (two image databases, 172 images) demonstrate that the proposed approach outperforms the existing methods considerably. The hybrid method yields the highest results: 100% accuracy for fair quality and 97.38 % for poor quality images.

As far as segmentation algorithms are concerned, SSHMC and SSVVPAAC on average outperform the benchmark methods. Both yield the highest PPV and sensitivity. Both achieve the same values of up of 82.45% for sensitivity on the fair set of images. Furthermore, SSHMC obtains the highest sensitivity of 70.67% for the poor set of images. SSVVPPAC

Finally, the proposed algorithm outperforms CTL, which is claimed the best, in terms of computational time, when the CTL is required to analyze a large area of an image and needs a large number of radial segments.

Acknowledgement

The authors would like to gratefully acknowledge financial support from Thailand Research Fund (TRF), grant number RSA5780034, the Center of Excellence in Biomedical Engineering of Thammasat University, and the Thai Royal Government Scholarship, the Ministry of Science and Technology, National Research University. We would also like to give thank the department of Ophthalmology Faculty of Medicine, Thammasat University for their help in providing the data collections.

References

[1] R. R. A. Bourne, P. Sukudom, P. J. Foster, V. Tantisevi, S. Jitapunkul, P. S. Lee, G. J. Johnson, and P. Rojanapongpun, “Prevalence of glaucoma in Thailand: a population based survey in Rom Klao District, Bangkok,” Br. J. Ophthalmol., vol. 87, no. 9, pp. 1069–1074, Sep. 2003.

[2] “WHO | Diabetes,” WHO. [Online]. Available: http://www.who.int/mediacentre/factsheets/fs312/en/. [Accessed date: 25-Jul-2016].

[3] T. J. MacGillivray, E. Trucco, J. R. Cameron, B. Dhillon, J. G. Houston, and E. J. R. van Beek, “Retinal imaging as a source of biomarkers for diagnosis, characterization and prognosis of chronic illness or long-term conditions,” Br. J. Radiol., vol. 87, no. 1040, p. 20130832, Jun. 2014.

[4] A. Hoover and M. Goldbaum, “Locating the optic nerve in a retinal image using the fuzzy convergence of the blood vessels,” IEEE Trans. Med. Imaging, vol. 22, no. 8, pp. 951–958, Aug. 2003.

[5] H. Li and O. Chutatape, “Automated feature extraction in color retinal images by a model based approach,” IEEE Trans. Biomed. Eng., vol. 51, no. 2, pp. 246–254, Feb. 2004.

[6] M. Lalonde, M. Beaulieu, and L. Gagnon, “Fast and robust optic disc detection using pyramidal decomposition and Hausdorff-based template matching,” IEEE Trans. Med. Imaging, vol. 20, no. 11, pp. 1193–1200, Nov. 2001.

[7] A. Dehghani, H. A. Moghaddam, and M.-S. Moin, “Optic disc localization in retinal images using histogram matching,” EURASIP J. Image Video Process., vol. 2012, no. 1, pp. 1–11, Oct. 2012.

[8] J. Lowell, A. Hunter, D. Steel, A. Basu, R. Ryder, E. Fletcher, and L. Kennedy, “Optic nerve head segmentation,” IEEE Trans. Med. Imaging, vol. 23, no. 2, pp. 256–264, Feb. 2004.

[9] R. J. Winder, P. J. Morrow, I. N. McRitchie, J. R. Bailie, and P. M. Hart, “Algorithms for digital image processing in diabetic retinopathy,” Comput. Med. Imaging Graph., vol. 33, no. 8, pp. 608–622, Dec. 2009.

[10] H. Li and O. Chutatape, “A model-based approach for automated feature extraction in fundus images,” in Proceedings of Ninth IEEE International Conference on Computer Vision, 2003, Vol.1, pp. 394–399.

[11] H. Li and O. Chutatape, “Boundary detection of optic disk by a modified ASM method,” Pattern Recognit., vol. 36, no. 9, pp. 2093–2104, Sep. 2003.

[12] S. Morales, V. Naranjo, J. Angulo, and M. Alcañiz, “Automatic Detection of Optic Disc Based on PCA and Mathematical Morphology,” IEEE Trans. Med. Imaging, vol. 32, no. 4, pp. 786–796, Apr. 2013.

[13] H.-K. Hsiao, C.-C. Liu, C.-Y. Yu, S.-W. Kuo, and S.-S. Yu, “A novel optic disc detection scheme on retinal images,” Expert Syst. Appl., vol. 39, no. 12, pp. 10600–10606, Sep. 2012.

[14] C. Sinthanayothin, J. F. Boyce, H. L. Cook, and T. H. Williamson, “Automated localisation of the optic disc, fovea, and retinal blood vessels from digital colour fundus images,” Br. J. Ophthalmol., vol. 83, no. 8, pp. 902–910, Aug. 1999.

[15] U. M. Akram and S. A. Khan, “Automated Detection of Dark and Bright Lesions in Retinal Images for Early Detection of Diabetic Retinopathy,” J. Med. Syst., vol. 36, no. 5, pp. 3151–3162, Nov. 2011.

[16] S. Lu, J. Liu, J. H. Lim, Z. Zhang, N. M. Tan, W. K. Wong, H. Li, and T. Y. Wong, “Automatic optic disc segmentation based on image brightness and contrast,” in Proceedings of SPIE Medical Imaging: Image Processing, 2010, Vol. 7623, p. 76234J–76234J–8.

[17] M. Esmaeili, H. Rabbani, A. M. Dehnavi, and A. Dehghani, “Automatic detection of exudates and optic disk in retinal images using curvelet transform,” IET Image Process., vol. 6, no. 7, pp. 1005–1013, Oct. 2012.

[18] M. Esmaeili, H. Rabbani, and A. M. Dehnavi, “Automatic optic disk boundary extraction by the use of curvelet transform and deformable variational level set model,” Pattern Recognit., vol. 45, no. 7, pp. 2832–2842, Jul. 2012.

[19] S. Shahbeig and H. Pourghassem, “Fast and automatic algorithm for optic disc extraction in retinal images using principle-component-analysis-based preprocessing and curvelet transform,” J. Opt. Soc. Am. A, vol. 30, no. 1, p. 13, Jan. 2013.

[20] C. Pereira, L. Gonçalves, and M. Ferreira, “Optic disc detection in color fundus images using ant colony optimization,” Med. Biol. Eng. Comput., vol. 51, no. 3, pp. 295–303, Nov. 2012.

[21] S. A. Ramakanth and R. V. Babu, “Approximate Nearest Neighbour Field based Optic Disk Detection,” Comput. Med. Imaging Graph., vol. 38, no. 1, pp. 49–56, Jan. 2014.

[22] A. Sopharak, B. Uyyanonvara, S. Barman, and T. H. Williamson, “Automatic detection of diabetic retinopathy exudates from non-dilated retinal images using mathematical morphology methods,” Comput. Med. Imaging Graph., vol. 32, no. 8, pp. 720–727, Dec. 2008.

[23] A. Azuara-Blanco, A. Harris, L. B. Cantor, M. M. Abreu, and M. Weinland, “Effects of short term increase of intraocular pressure on optic disc cupping,” Br. J. Ophthalmol., vol. 82, no. 8, pp. 880–883, Aug. 1998.

[24] X. Zhu, R. M. Rangayyan, and A. L. Ells, “Detection of the Optic Nerve Head in Fundus Images of the Retina Using the Hough Transform for Circles,” J. Digit. Imaging, vol. 23, no. 3, pp. 332–341, Feb. 2009.

[25] S. Lu, “Accurate and Efficient Optic Disc Detection and Segmentation by a Circular Transformation,” IEEE Trans. Med. Imaging, vol. 30, no. 12, pp. 2126–2133, Dec. 2011.

[26] D. Welfer, J. Scharcanski, C. M. Kitamura, M. M. Dal Pizzol, L. W. B. Ludwig, and D. R. Marinho, “Segmentation of the optic disk in color eye fundus images using an adaptive morphological approach,” Comput. Biol. Med., vol. 40, no. 2, pp. 124–137, Feb. 2010.

[27] A. A. H. A. R. Youssif, A. Z. Ghalwash, and A. A. S. A. R. Ghoneim, “Optic Disc Detection From Normalized Digital Fundus Images by Means of a Vessels’ Direction Matched Filter,” IEEE Trans. Med. Imaging, vol. 27, no. 1, pp. 11–18, Jan. 2008.

[28] A. E. Mahfouz and A. S. Fahmy, “Fast Localization of the Optic Disc Using Projection of Image Features,” IEEE Trans. Image Process., vol. 19, no. 12, pp. 3285–3289, Dec. 2010.

[29] E. J. Carmona, M. Rincón, J. García-Feijoó, and J. M. Martínez-de-la-Casa, “Identification of the optic nerve head with genetic algorithms,” Artif. Intell. Med., vol. 43, no. 3, pp. 243–259, Jul. 2008.

[30] A. Giachetti, L. Ballerini, and E. Trucco, “Accurate and reliable segmentation of the optic disc in digital fundus images,” J. Med. Imaging, vol. 1, no. 2, pp. 024001–024001, 2014.

[31] A. Aquino, M. E. Gegundez, and D. Marin, “Automated optic disc detection in retinal images of patients with diabetic retinopathy and risk of macular edema,” Int. J. Biol. Life Sci., vol. 8, no. 2, pp. 87–92, 2012.

[32] K. Akita and H. Kuga, “A computer method of understanding ocular fundus images,” Pattern Recognit., vol. 15, no. 6, pp. 431–443, Jan. 1982.

[33] R. Chrastek, M. Skokan, L. Kubecka, M. Wolf, K. Donath, J. Jan, G. Michelson, H. Niemann, and others, “Multimodal retinal image registration for optic disk segmentation,” Methods Inf. Med., vol. 43, no. 4, pp. 336–342, 2004.

[34] D. Kavitha and S. S. Devi, “Automatic detection of optic disc and exudates in retinal images,” in Proceedings of 2005 International Conference on Intelligent Sensing and Information Processing, 2005, pp. 501–506.

[35] M. Foracchia, E. Grisan, and A. Ruggeri, “Detection of optic disc in retinal images by means of a geometrical model of vessel structure,” IEEE Trans. Med. Imaging, vol. 23, no. 10, pp. 1189–1195, Oct. 2004.

[36] M. Niemeijer, M. D. Abràmoff, and B. van Ginneken, “Fast detection of the optic disc and fovea in color fundus photographs,” Med. Image Anal., vol. 13, no. 6, pp. 859–870, Dec. 2009.

[37] A. Dehghani, M.-S. Moin, and M. Saghafi, “Localization of the optic disc center in retinal images based on the Harris corner detector,” Biomed. Eng. Lett., vol. 2, no. 3, pp. 198–206, Oct. 2012.

[38] D. Zhang and Y. Zhao, “Novel Accurate and Fast Optic Disc Detection in Retinal Images With Vessel Distribution and Directional Characteristics,” IEEE J. Biomed. Health Inform., vol. 20, no. 1, pp. 333–342, Jan. 2016.

[39] A. M. Mendonça, A. Sousa, L. Mendonça, and A. Campilho, “Automatic localization of the optic disc by combining vascular and intensity information,” Comput. Med. Imaging Graph., vol. 37, no. 5–6, pp. 409–417, Jul. 2013.

[40] A. S. Semashko, A. S. Krylov, and A. S. Rodin, “Using Blood Vessels Location Information in Optic Disk Segmentation,” in Image Analysis and Processing – ICIAP 2011, G. Maino and G. L. Foresti, Eds. Springer Berlin Heidelberg, 2011, pp. 384–393.

[41] R. M. Rangayyan, X. Zhu, F. J. Ayres, and A. L. Ells, “Detection of the Optic Nerve Head in Fundus Images of the Retina with Gabor Filters and Phase Portrait Analysis,” J. Digit. Imaging, vol. 23, no. 4, pp. 438–453, Jan. 2010.

[42] J. Staal, M. D. Abramoff, M. Niemeijer, M. A. Viergever, and B. van Ginneken, “Ridge-based vessel segmentation in color images of the retina,” IEEE Trans. Med. Imaging, vol. 23, no. 4, pp. 501–509, Apr. 2004.

[43] Hoover, A and Goldbaum, M., “The STructure Analysis of the REtina (STARE) project.” San Diego, US. Retrieved February 18, 2013, from http://www.ces.clemson.edu/~ahoover/stare.

[44] N. Muangnak, P. Aimmanee, S. Makhanov, and B. Uyyanonvara, “Vessel transform for automatic optic disk detection in retinal images,” IET Image Process., vol. 9, no. 9, pp. 743–750, 2015.
[45] C. Duanggate, B. Uyyanonvara, S. S. Makhanov, S. Barman, and T. Williamson, “Parameter-free optic disc detection,” Comput. Med. Imaging Graph., vol. 35, no. 1, pp. 51–63, Jan. 2011.
[46] J. a. K. Suykens and J. Vandewalle, “Least Squares Support Vector Machine Classifiers,” Neural Process. Lett., vol. 9, no. 3, pp. 293–300.
[47] S. Chucherd, A. Rodtook, and S. S. Makhanov, “Phase Portrait Analysis for Multiresolution Generalized Gradient Vector Flow,” IEICE Trans. Inf. Syst., vol. E93-D, no. 10, pp. 2822–2835, Oct. 2010.
[48] A. Witkin, “Scale-space filtering: A new approach to multi-scale description,” in Proceedings of Acoustics, Speech, and Signal Processing, IEEE International Conference on ICASSP ’84., 1984, Vol. 9, pp. 150–153.
[49] T. Lindeberg, Scale-Space Theory in Computer Vision. Springer Science & Business Media, 2013.
[50] C-C. Chang and C-J. Lin, “LIBSVM: a library for support vector machines,” ACM Trans. Intell. Syst. Technol., vol. 2, pp. 1–27, 2011.
[51] S. Sekhar, W. Al-Nuaimy, and A. K. Nandi, “Automated localisation of retinal optic disk using Hough transform,” in Proceedings of the 5th IEEE International Symposium on Biomedical Imaging: From Nano to Macro, 2008, pp. 1577–1580.
[52] S. Ravishankar, A. Jain, and A. Mittal, “Automated feature extraction for early detection of diabetic retinopathy in fundus images,” in Proceedings of IEEE Conference on Computer Vision and Pattern Recognition (CVPR 2009), 2009, pp. 210–217.
[53] D. Welfer, J. Scharcanski, and D. R. Marinho, “A morphologic two-stage approach for automated optic disk detection in color eye fundus images,” Pattern Recognit. Lett., vol. 34, no. 5, pp. 476–485, Apr. 2013.

<u>เอกสารแนบหมายเลข 3</u>

Output จากโครงการวิจัยที่ได้รับทุนจาก สกว.

1. ผลงานตีพิมพ์ในวารสารวิชาการนานาชาติ

Nittaya Muangnak, Pakinee Aimmanee, Stanislav S. Makhanov, and Bunyarit Uyyanonvara (2015). Vessel transform for automatic optic disk detection in retinal images, IET Image Processing, Vol. 9, No. 9, September 2015, pp. 743-750.

2. การนำผลงานวิจัยไปใช้ประโยชน์

- **เชิงพาณิชย์**

  ไม่มี

- **เชิงนโยบาย**
  ไม่มี
- **เชิงสาธารณะ (มีเครือข่ายความร่วมมือ/สร้างกระแสความสนใจในวงกว้าง)**
  ได้เครือข่ายความร่วมมือระหว่างสถาบันเทคโนโลยีนานาชาติสิรินธร มหาวิทยาลัยธรรมศาสตร์ กับศูนย์ตาโรงพยาบาลธรรมศาสตร์ ที่มีความสนใจร่วมกันในการทำเอาเทคโนโลยีการประมวลผลภาพมาช่วยต่อยอดแก้ปัญหาวิจัยในจักษุคลีนิค
- **เชิงวิชาการ (มีการพัฒนาการเรียนการสอน/สร้างนักวิจัยใหม่)**
  ได้ผลิตนักศึกษาปริญญาเอกจำนวน 1 คนและปริญญาโท 1 คน

3. อื่น ๆ (เช่น ผลงานตีพิมพ์ในวารสารวิชาการในประเทศ การเสนอผลงานในที่ประชุมวิชาการ หนังสือ การจดสิทธิบัตร)

ได้ตีพิมพ์ผลงานในวารวารวิชาการระดับนานาชาติ

ภาคผนวก

Reprint บทความสำหรับการเผยแพร่

IET Image Processing

Research Article

IET Journals
The Institution of Engineering and Technology

Vessel transform for automatic optic disk detection in retinal images

ISSN 1751-9659
Received on 4th August 2014
Accepted on 26th February 2015
doi: 10.1049/iet-ipr.2015.0030
www.ietdl.org

Nittaya Muangnak, Pakinee Aimmanee, Stanislav Makhanov ✉, *Bunyarit Uyyanonvara*

Sirindhorn International Institute of Technology, Thammasat University, 131 Moo 5, Tiwanont Road, Bangkadi, Muang, Pathumthani 12000, Thailand
✉ *E-mail: makhanov@siit.tu.ac.th*

Abstract: Precise localisation of an optic disk (OD) in the retinal images is one of the most important problems in the ophthalmic image processing. Although a considerable progress has been made towards a computerised solution of the problem, the numerical algorithms often fail on retinal images characterised by poor quality. Therefore, the authors propose a new method suitable for low-quality images based on exploiting the convergence of the blood vessels to the OD. The novelty of the proposed techniques includes clustering the vessels endowed with a novel correction procedure and the vessel transform (VT) which measures the distance to the main clusters. The algorithm is integrated into the scale-space (SS) analysis to detect the boundary of the OD. The integrated method is called SS algorithm with VT (SSVT). SSVT has been tested on retinal images from two databases with fair and poor images against the fuzzy convergence (FC) method and a modification of the circular transform proposed by Lu. The absolute improvement on sensitivity of SSVT against FC and Lu's are up to 12.37% and 8.18%. Bigger improvements of SSVT in terms of positive predictive value are up to 37.46% and 30.84% against FC and Lu's, respectively.

1 Introduction

Precise automatic localisation of an optic disk (OD) in the retinal images is an important problem in the ophthalmic image processing. Once the OD has been identified, many other regions of clinical importance such as the fovea or macula can be easily detected and/or localised. The OD is also important for establishing a frame of reference within the retinal image. The OD usually appears in the retinal images as a bright, yellowish, circular or oval object, roughly one-sixth the width of the image in diameter [1]. Any irregularity in the appearance of the OD is a sign of abnormalities or diseases such as glaucoma, diabetic retinopathy (DR) or hypertensive retinopathy [2].

Nowadays, one in ten people is advised for annual retinal screening because of a variety of medical conditions [3]. However, annual retinal screening is nearly impossible especially in developing countries because of the huge gap between the number of professional ophthalmologists and the patients. This implies the necessity of automatic screening systems to assist the ophthalmologists in diagnosing the early stage of diseases such as glaucoma and DR using computer-based identification. Since the eye fundus imaging is a frequent clinical procedure, the retinal images are commonly used for a preliminary diagnosis and detecting suspicious cases.

The conventional OD segmentation usually employs a suitable set of features such as brightness, shape, size and the variation of the grey level (entropy) and template matching. Lalonde *et al.* [4] localised the OD by using a pyramidal decomposition based on Haar discrete wavelet transform and segmented the OD using a Hausdorff-based template matching. Li and Chutatape [5] localised the OD by the principal component analysis (PCA) and detected the OD's boundary using an iterative searching procedure called the active shaped model. Lowell *et al.* [6] performed a specialised template matching, and segmentation by using an active contour (snake). Lu *et al.* [3] employed brightness and texture to form a model template. The OD region is determined by a pair of morphological operations and an ellipse is fitted to the detected OD region. Akram and Khan [7] employed the intensity variation and the grey levels as the major features characterising the OD. Curvelet transform has also been applied to solve OD segmentation problem in [8, 9]. Shahbeig and Hossein [10] combined the curvelet transform with the PCA and morphological operators based on geodesic conversions to obtain the OD region. Pereira *et al.* [11] analysed the brightness of a series of blurred images and applied the ant colony optimisation preceded by an anisotropic diffusion filter. Morales *et al.* [12] also used PCA combined with centroid calculation, stochastic watershed and region discrimination. Dehghani *et al.* [13] used histograms of each colour component. Hsiao *et al.* [14] localised the OD by an illumination correction algorithm and segmented the OD contour by using a supervised gradient vector flow snake model. Ramakanth and Babu [15] proposed the OD localisation based on approximate nearest neighbour field. Using the fact that OD appears as a bright region, Pourreza-Shahri *et al.* [16] detected it by using radon transformation of multiple overlapping windows.

One of the most successful works tested against many existing algorithms is Lu [17]. The proposed modification of the circular transform combined with evaluation of the brightness is claimed to be more efficient, more accurate and faster than other state-of-the-art techniques: a morphological approach proposed by Welfer *et al.* [18], a vessel's direction matched filter proposed by Youssif *et al.* [19], localisation using dimensionality reduction of the search space proposed by Mahfouz and Fahmy [20] and genetic algorithms by Carmona *et al.* [21].

The major drawback of the feature-based approaches is that they often incorrectly localise the OD when the OD's physical appearances such as shape, colour, brightness or size become abnormal. The OD obscured by blood vessels or only partially visible (blur, shadows and noise) could be also misclassified. Besides, the feature-based methods could be highly sensitive to distractors which often appear in the retinal images [6].

In the meantime, a powerful subclass of the OD detection algorithms based on the location of the vascular structures is often overlooked. Only a few papers exploit the convergence of the blood vessels to the OD. Akita and Kuga [22] traced the parent–child relationship between blood vessels segments, tracking back

to the centre of the OD. In addition to brightness and shape features of the OD, Chrastek *et al.* [23] checked the area where vertically oriented vessels converge. Foracchia *et al.* [24] used the fact that all retina vessels originate from the OD and their paths follow a similar directional pattern (parabolic course). To describe the general direction of retinal vessels, a geometrical parametric model was proposed, where two of the model parameters are the coordinates of the OD centre. Niemeijer *et al.* [25] approximated the location of the OD using *k*-nearest neighbour regression. Dehghani *et al.* [26] localised the OD by detecting the region having the highest number of vessels, corners and bifurcation points. Welfer *et al.* [27] and Zhang and Zhao [28] used the assumption that the vascular network is alligned horizontally in the retina image. Both work first segmented and skeletonised the network of vessels and checked for the point where the main vessels arcade fragment was intercepted by the horizontal line to obtain the approximated location of OD. The major drawback of this approach is that it is not rotationally invariant. Mendonca *et al.* [29] use the entropy of vascular directions to quantify occurrences and the diversity of vessel orientations of each pixel. Dashtbozorg *et al.* [30] extended this idea using a multi-resolution sliding band filter.

One of the most successful vessel convergence techniques are introduced by Hoover and Goldbaum [1]. The method employing the vessel convergence as the primary feature is based on the fuzzy convergence (FC) endowed with a voting scheme. The voting takes place on the integer grid of the original image. Each vessel is represented by a fuzzy segment, whose area contributes votes to its pixels. The summation of votes at each pixel produces an image map representing the strength of the convergence of each pixel. The map is then blurred and thresholded to produce points of the strongest convergence. The FC techniques have been applied on multiple scales and combined with a feature-based approach employing the equalised brightness. The verification of the method on STructured Analysis of the Retina (STARE) database shows the highest performance overall (89%), and a complete success on the healthy retina test cases (100%). Nonetheless, the method does not consider the hierarchical structure of the vessels and their importance. As a matter of fact, the vessel network consists of the main vessels and several levels of secondary vessels.

The main vessels converge to the OD, whereas the secondary vessels are positioned randomly with regard to the OD. Therefore the vascular network can be thought of as a collection of clusters of connected conduits similar to the river networks. The clusters converge to the OD in the sense that points belonging to the OD are closer to each cluster than points not belonging to OD. This concept is not always true if we consider convergence of individual vessels. It is not hard to give an example where the secondary vessels converge to a false OD.

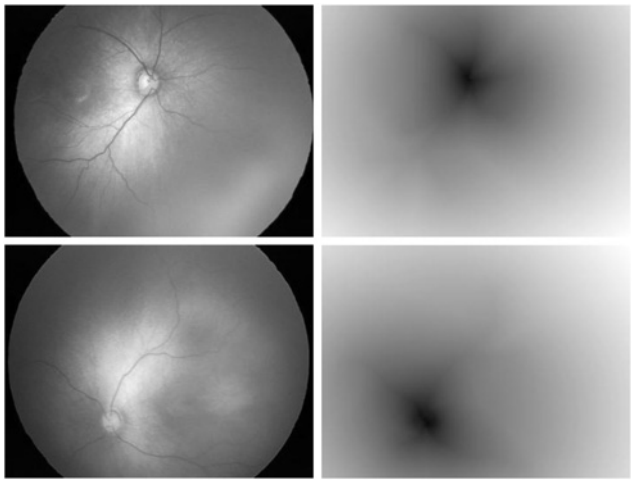

Fig. 1 *Original retinal images (left) and their corresponding VTs (right)*

Therefore we propose new techniques based on clustering of the vessels and a transform which measures the distance to the main vessel clusters. The vessel transform (VT) is generated using a hierarchical clustering combined with a special correction procedure to test the validity of the clusters. The algorithm is integrated into the scale-space (SS) analysis. The new algorithm has been tested on poor quality retinal images from two databases (172 images) against the FC method [1], and a recent modification of the circular transform [17]. Furthermore, the space scale boundary detection [31] was tested with and without the VT option. The numerical experiments demonstrate that the proposed algorithm outperforms the benchmark methods in terms of the correct localisation of the OD and improves segmentation of the OD based on the space scale scheme.

2 Vessel transform

The VT is given by

$$V(p) = \frac{1}{N}\sum_{i=1}^{N} \mathrm{dist}(p,\ c_i) \tag{1}$$

where c_i is the i^{th} cluster of vessels, N is the number of clusters, $p = (x,\ y)$ is an arbitrary point in the image and $\mathrm{dist}(p,\ c) = \min_{p' \in c} ||p - p'||$. An introductory example in Fig. 1 displays sample retinal images and the corresponding VTs. The dark part of the VT image corresponding to the vessel convergence region locates the OD.

Clearly, our approach requires a reliable and accurate vessel segmentation method. At the moment, there exist numerous vessel segmentation algorithms applicable to variety of retinal images [32–35]. Our numerical experiments with available source codes revealed a good performance of the automated retinal image analyser [35, 36] developed by the Centre for Vision and Vascular Science of Queen's University of Belfast. The method is based on thresholding of wavelet coefficients on different spatial scales and vessel location refinement using the centreline spline fitting. The method is unsupervised and does not use any masks or filters since they often must be tailored for a particular type or resolution of image and require modifications to be applied to others. As opposed to that the choice of wavelet levels and thresholds does not need to be changed for similar images. Following [35, 36], we set the wavelet coefficients threshold to identify the lowest 20% of coefficients as vessels. Although this typically produces an oversegmented image, small isolated objects and holes inside the vessels can be easily removed by morphological operations.

The input of the clustering algorithm is a collection of vessels (v_1, v_2, …, v_m). Each vessel is represented by the Cartesian coordinates: $v_i = ((x,\ y)_{i,1},\ (x,\ y)_{i,2},\ \ldots,\ (x,\ y)_{i,N_i})$. The first step is pre-processing designed to remove the outliers: short, thin and faint vessels. It requires the following thresholds: T_{l} is the length threshold, T_{t} is the thickness threshold, T_f is the threshold on the grey-level intensity of the vessel relative to the background. The second step merges the vessels into clusters and removes the isolated vessels. The merging step employs a threshold T_{d} on the maximum distance between clusters which can be merged into a new cluster. We apply a classical hierarchical bottom-up clustering endowed with an original correction procedure. Initially, the algorithm treats each vessel as a singleton $c_i = v_i$. Next, it successively merges clusters c_i, c_j if $\mathrm{dist}(c_i,\ c_j) < T_{\mathrm{d}}$ until they have been merged into several well separated sets. The post-processing procedure detects and removes the outliers (small clusters) by using the condition $N_{c_i} < T_L$, where N_{c_i} denotes the size of the cluster and T_L denotes the corresponding threshold.

Note that clustering does not include time-consuming tracing procedures designed to detect the tree-like structures of the vessels. However, if trained, the algorithm returns well separated clusters sufficient to generate a VT which localises the

IET Image Process., 2015, Vol. 9, Iss. 9, pp. 743–750

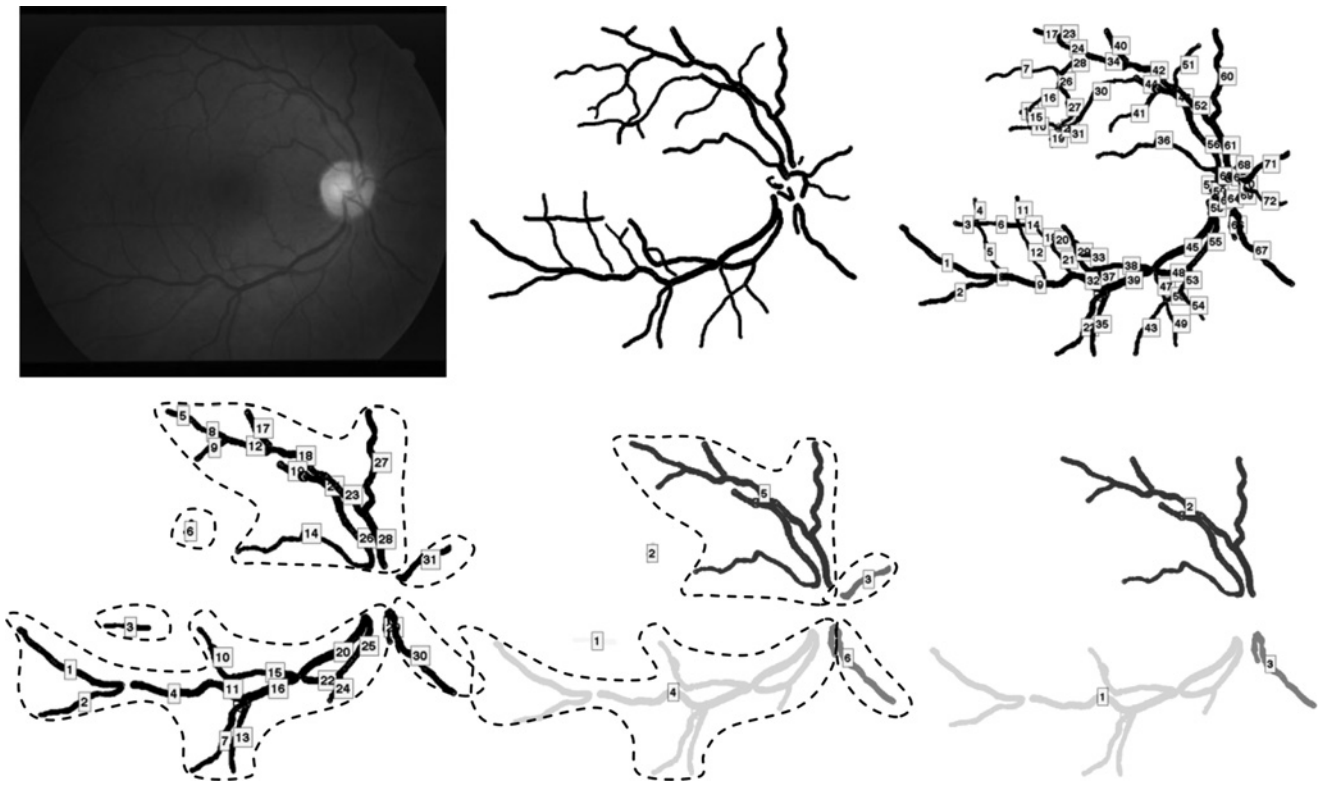

Fig. 2 *Original image (top left), extracted vessels (top middle), segmented vessels (top right), removing short, thin and faint vessels (bottom left), removing small clusters (bottom middle), final clusters (bottom right)*

convergence region and consequently the OD. Fig. 2 illustrates the proposed clustering method.

3 Correction algorithm

The VT-based segmentation of the OD requires that the resulting clusters converge to the OD. Therefore for the vessel networks separated into three or more clusters, we verify the quality of convergence as follows. First, we evaluate the convergence region $\Omega = \arg\min_p V(p)$ and its centroid. Next, we withdraw the clusters one by one from the collection and evaluate the convergence regions Ω' corresponding to these new collections. If for some Ω′, $\text{dist}(O_\Omega, O_{\Omega'}) > T_\Omega$, where O_Ω is the centroid of Ω, O'_Ω is the centroid of Ω′ and T_Ω is the corresponding threshold, the clustering is discarded. Our assumption is that if the vessels strongly converge to Ω, the system without one cluster converges approximately to the same region (see Fig. 3).

Furthermore, if $\min_{c_i}(\text{dist}(c_i, \Omega_c)) < T_{VT}$, where T_{VT} is the corresponding threshold and c_i is the i^{th} cluster and Ω_c is the centroid of Ω (the cluster is close enough to the convergence region), the clustering is considered successful. In this case, the VT is included in the prescribed set of features for a further evaluation.

4 Threshold selection

The proposed method requires the following thresholds: T_l is the minimal acceptable length of the vessel for a particular image (shorter vessels will be eliminated), T_t is the minimal acceptable thickness, T_f is the maximum acceptable intensity of the vessel relative to the background, T_d is the maximum distance between the clusters which can be merged into a new cluster, T_L is the minimum acceptable size of the cluster and T_Ω, T_{VT} used by the convergence test (see Section 3). The thresholds are obtained using a bivariate quadratic approximation given by

$$T(\mu, \sigma) = a_1\mu^2 + a_2\sigma^2 + a_3\mu + a_4\sigma + a_5\mu\sigma + a_6 \quad (2)$$

where μ and σ are the mean and the standard deviation of the corresponding parameter evaluated for a particular image. For instance, $T_l \equiv T_l(\mu_l, \sigma_l)$ is the threshold on the minimal acceptable length of the vessel, whereas μ_l is the mean length of a vessel in a particular image and σ_l is the standard deviation (see Fig. 7).

5 SS algorithm with VT

The VT method with the improvements described in Sections 2–4 generated an approximated location of the OD but it has not yet detected the boundary of the OD. To obtain the OD's rim, we

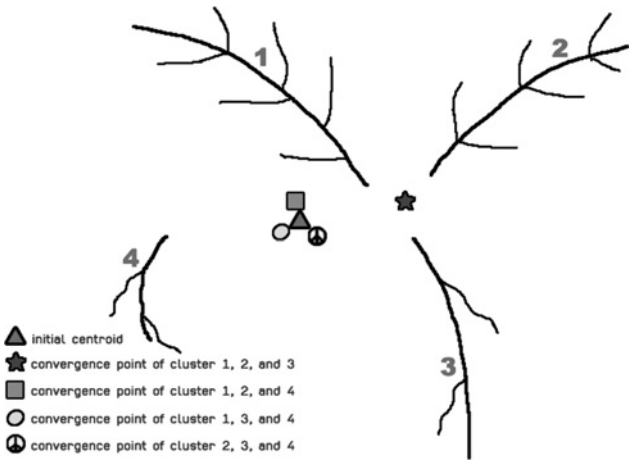

Fig. 3 *Convergence test*

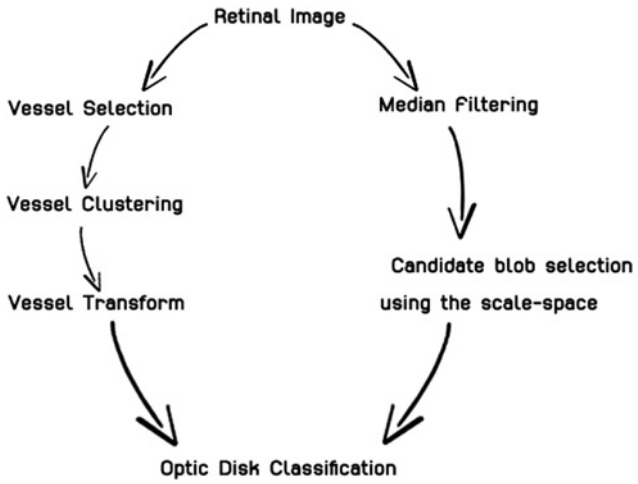

Fig. 4 *VT combined with the SS segmentation*

integrate our approach into the SS boundary detection algorithm proposed by Duanggate *et al.* [31]. The modified algorithm is called the space scale algorithm with the VT (SSVT). Fig. 4 shows the proposed integration of SS and VT into the SSVT.

The SS approach is based on the original theory proposed by Lindeberg [37] in 1994. The image is converted into a one-parameter family of smoothed images. Objects (blobs) which appear stable under smoothing at different scales along with their features such as the size, the compactness, the entropy, the average intensity etc. are considered as the OD candidates. We modify the SS algorithm by adding the VT score as an additional feature. To integrate the feature in the SS method, we use an automatic decision tree generator available from the Waikato Environment for Knowledge Analysis [38]. The examples of the decision trees are given in Section 7.

6 Experimental setup

We tested the proposed method against the existing techniques on two collections of images, that is, the STARE [39] which is a standard collection available on the internet and a dataset originally collected to detect the signs of retinopathy of prematurity (ROP) by Dr. Sarah Barman with Kingston University of UK. All digital retinal images from ROP were taken from patients with non-dilated pupils using a KOWA-7 non-mydriatic retinal camera with a 45° field of view. The images were stored in JPEG format 640 × 480 pixels at 24 bits per pixel.

To reduce the inconsistency between human experts, the ground truth was obtained from three ophthalmologists from Thammasat University Hospital, Thailand. The ophthalmologists were asked to hand-draw the OD rims on each retina image from two collections three times. To check the inter-observer variability and intra-observer variability, we used the voting overlapping score defined as the ratio of an area in the image that at least two ground truths agree on that it is part of OD to the area obtained from the union of the three ground truth contours. The inter-observer variability values of the experts are 0.86 and 0.91 for the ROP and STARE collections, respectively. The intra-observer variabilities of each expert are 0.92 and 0.93 on average for the ROP and STARE collections, respectively.

Images with bright, round and clear border of the ODs were classified visually as 'fair', the rest is considered 'poor'. There are 60 images with fair quality and 31 images with poor quality for the ROP collection, whereas 31 images with fair quality and 50 images with poor quality for the STARE collection. Figs. 5*a* and 5*b* display examples of 'fair' and 'poor' images.

Our two collections of test images have been obtained by different devices with different lighting conditions. Therefore, they require different sets of thresholds which are obtained by the quadratic regression (2). Fig. 6 illustrates the proposed threshold selection. We train the method using the classic 70–30% ratio between the training and the testing data.

To combine features in SS method, we use an automatic decision tree generation available from the Waikato Environment for Knowledge Analysis [38]. Features evaluated for the candidate blob in scaled space are the size (s), the compactness (c), the entropy (e), the average intensity (i) and the average value of the VT (V). The resulting decision trees and the particular thresholds are shown in Fig. 7.

Note that the decision trees indicate the importance of V, s and c, whereas the branches including the entropy and the intensity have been automatically pruned. The forthcoming Section 7 shows how the VT improves the accuracy of the classification.

7 Experiments and results

In this section, we show and analyse results of applying the proposed algorithm to the ROP and STARE collections of retinal images. We

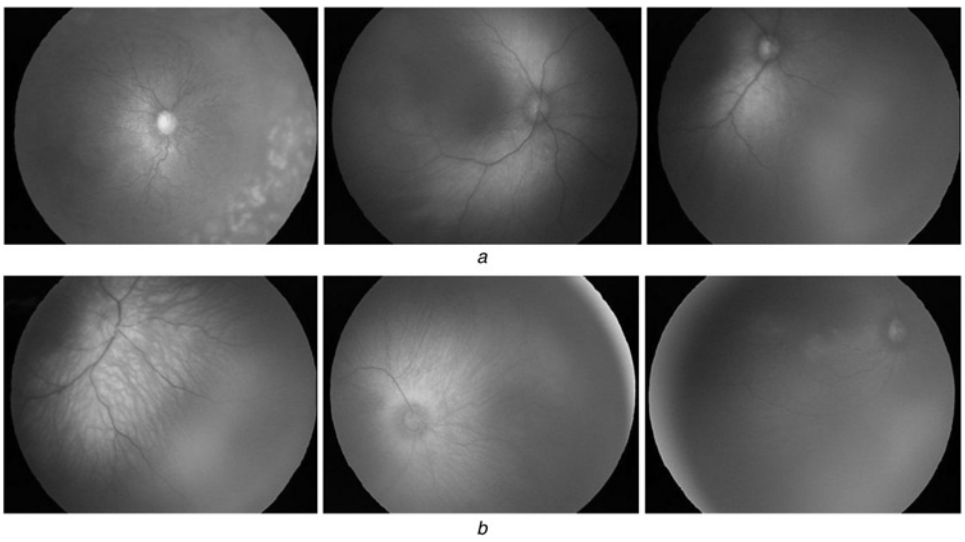

Fig. 5 *Examples of the 'fair' and the 'poor' images*

a Fair images
b Poor images

IET Image Process., 2015, Vol. 9, Iss. 9, pp. 743–750

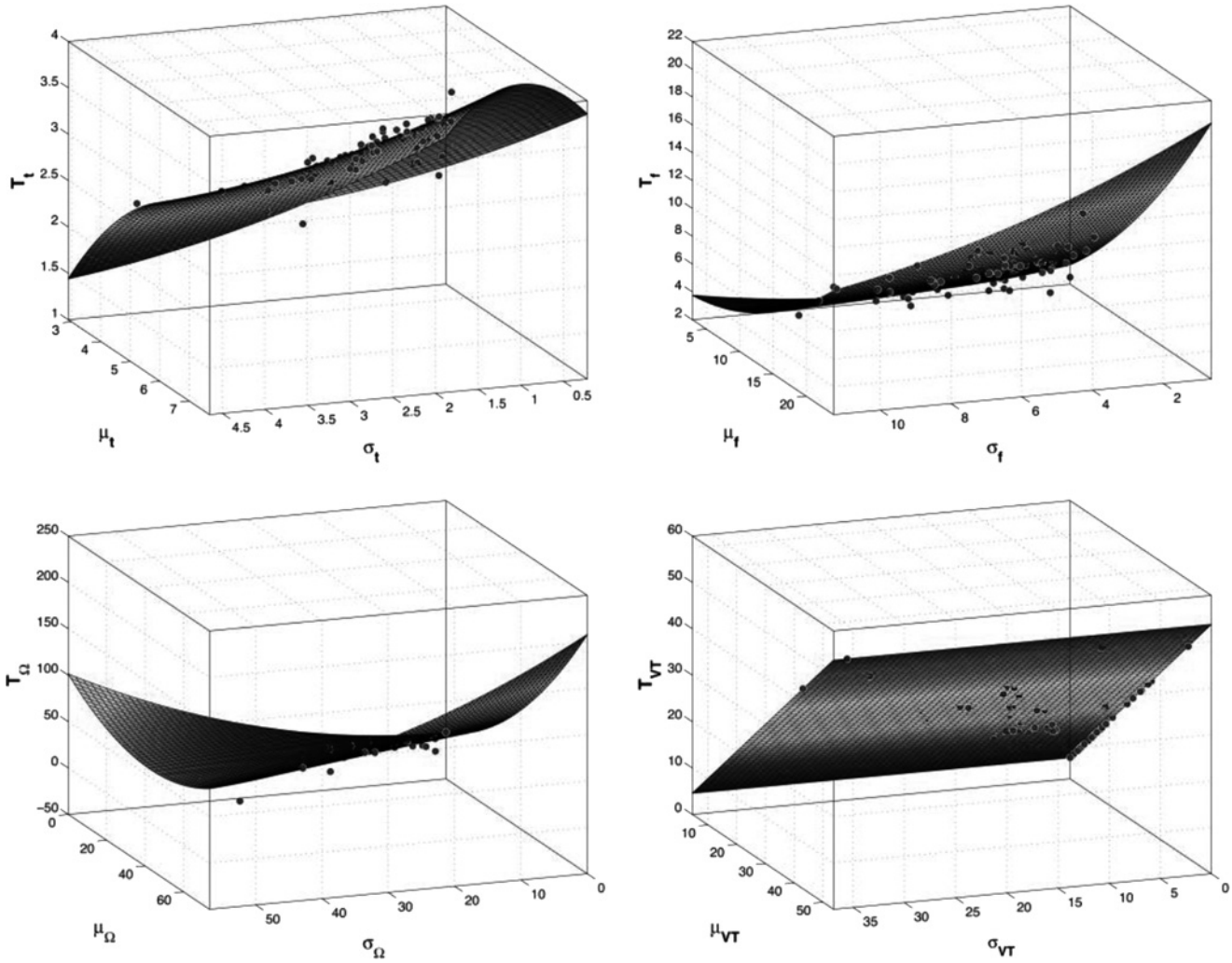

Fig. 6 *Example of quadratic regression applied to the STARE collection*

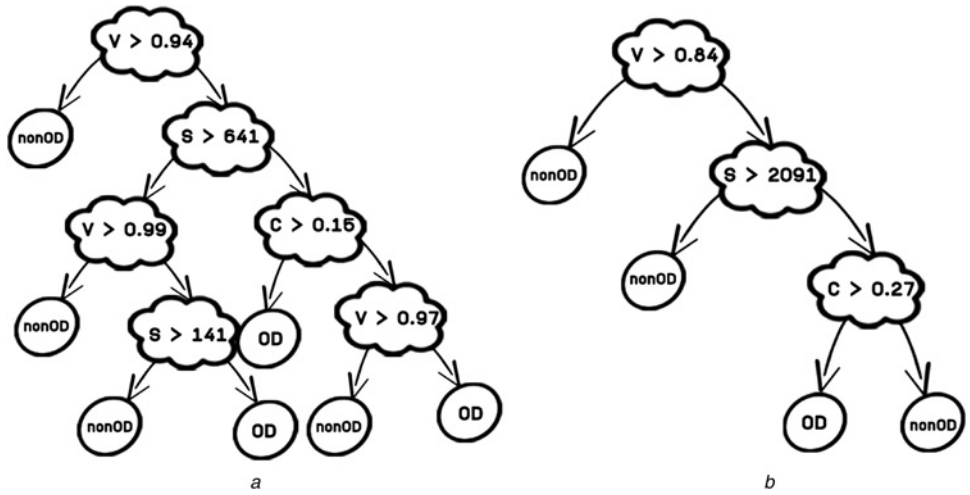

Fig. 7 *Decision trees for test collections*

a ROP collection
b STARE collection

test the method against FC method [40] and a recent modification of the circular transform proposed in [17]. Furthermore, we compare the standard SS segmentation [31] and the SS method endowed with the proposed VT.

7.1 Performance of the VT in locating the OD

We applied and compared the performance of VT with the advanced version of the circular transform Lu's method [17] and FC method [1]. Fig. 8 shows introductory examples when Lu's method or/and

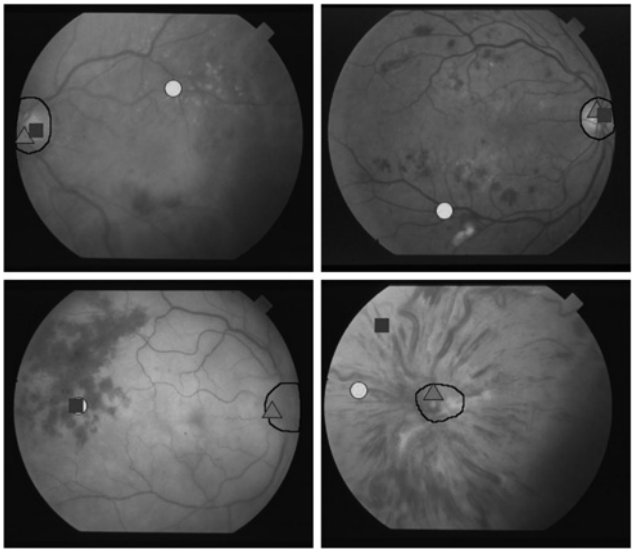

Fig. 8 *OD location: ground truth – solid line, VT – triangle, FC – circle and Lu's – square*

FC fail, whereas the proposed method indicates the correct OD location.

The accuracy of the OD locating was evaluated as follows. If the convergence region Ω (see Section 3) is contained entirely inside the ground truth contour, we consider it a correct location of the OD. Lu's method was considered successful if the centroid of the circular transform contour was located inside the ground truth contour.

Table 1 shows the accuracy of the location of the OD location for the fair and poor images processed by the VT, FC and Lu on the STARE collection. The VT outperforms FC for both the groups with the absolute improvement of about 6%. However, Lu's method is slightly better. This is because of the better quality of the images in that database. However, the VT performs much better on fair and poor quality images from ROP database as follows: fair images: Lu's-88%, VT-95% and poor images: Lu's-64.5%, VT-96.7%.

Furthermore, the advanced circular transform of Lu claims to be the fastest and the most accurate as compared with line operator method [18], geometrical model method [19], the vessel direction matched filter [20] and the dimensionality reduction method [21]. Therefore we conjecture that our proposed algorithm should outperform the above-mentioned procedures for the poor images as well.

7.2 Performance of the SSVT in detecting the OD region

Next, we combine our approach with the SS algorithm for detecting the OD proposed by Duanggate *et al.* [31]. We extend the SS algorithm by adding the VT score as an additional feature. The modified algorithm is called the SSVT. Our OD classification is performed using a decision tree which includes the above-mentioned features along with the VT-feature. As opposed to the previous section where the location of the OD was evaluated by finding the centroid of the convergence area, the OD region is now determined by using a combination of the SS which generates the candidate blobs and the proposed decision tree (Fig. 7).

We evaluate the performance using two standard schemes: sensitivity and positive predictive value (PPV). The first one reveals the accuracy while the second one reflects completeness of the obtained solution. The sensitivity is defined to be the ratio of the number of pixels detected correctly as OD to the total number of pixels detected as OD. The PPV is the ratio of number of pixels detected correctly as OD to the total number of pixels of OD from the ground truth.

The algorithms were tested on the ROP and the STARE collections. Fig. 8 shows examples when SSVT outperforms the other two approaches. The VT-feature has a strong impact on the blob classification process. In many cases, the SS and Lu fail to detect the OD because of insufficient information provided by the basic features. As opposed to that, SSVT employs the convergence of the vessels which is not sensitive to the variation of the contrast and the noise as long as the entire vascular network or at least a major part of it has been correctly detected and clustered.

The tests of the performance of the SSVT against the SS and Lu's are presented in Table 2. The bold values represent the best result in a particular category. The SSVT outperforms SS and Lu's in 'both quality measures for each group of the images (fair and poor) and for each collection of data'. In particular, when the image quality is poor, the SSVT outperforms the other two approaches in terms of PPV considerably (Table 3).

For the fair images, the advantages of the SSVT over SS in average sensitivity are up to 2.09% (STARE) and 4.45% (ROP). The SSVT underperforms Lu's in average sensitivity by 10.19% (STARE) but outperforms Lu's by 8.18%. For the poor images,

Table 1 Accuracy of the OD location

Collections	Image quality	Accuracy, %			Absolute improvement VT against FC, %	Absolute improvement VT against Lu's, %
		FC	VT	Lu's		
ROP	fair	N/A	95	88.33	N/A	6.68
	poor	N/A	96.77	64.52	N/A	32.25
STARE	fair	90.32	96.77	100	6.45	–3.23
	poor	88	94	98	6	–4
average (STARE only)		89.16	95.39	98.77	6.23	–3.38
average (ROP only)		N/A	95.89	76.42	N/A	19.47

VT against FC and Lu's circular transform.

Table 2 Average sensitivity and PPV of SS and Lu's against SSVT

Collections	Image quality	Average sensitivity			Average PPV		
		Lu's	SS	SSVT (SSVT-Lu's, SSVT-SS)	Lu's	SS	SSVT (SSVT-Lu's, SSVT-SS)
ROP	fair	74.29	80.39	**82.47** (+8.18, +2.08)	66.42	86.08	**87.41** (20.99, 1.33)
	poor	**61.28**	45.51	58.18 (–3.1, 12.67)	46.39	53.01	**83.85** (37.46, 30.84)
STARE	fair	**72.59**	57.95	62.4 (–10.19, 4.45)	**84.66**	67.09	74.14 (–10.52, 7.05)
	poor	41.23	43.27	**45.76** (4.53, 2.49)	69.89	59.18	**74.59** (4.7, 15.41)
average		62.35	62.2	**64.26** (1.91, 2.06)	66.84	66.34	**80** (13.16, 13.66)

IET Image Process., 2015, Vol. 9, Iss. 9, pp. 743–750

Table 3 Computational time Lu's against SSVT

Percentage of test pixels, %	Number of radial line segments	Average time Lu's, min	Average time SSVT, min
20	40	1.57	4.85
20	180	6.63	
60	40	4.29	
60	180	18.84	

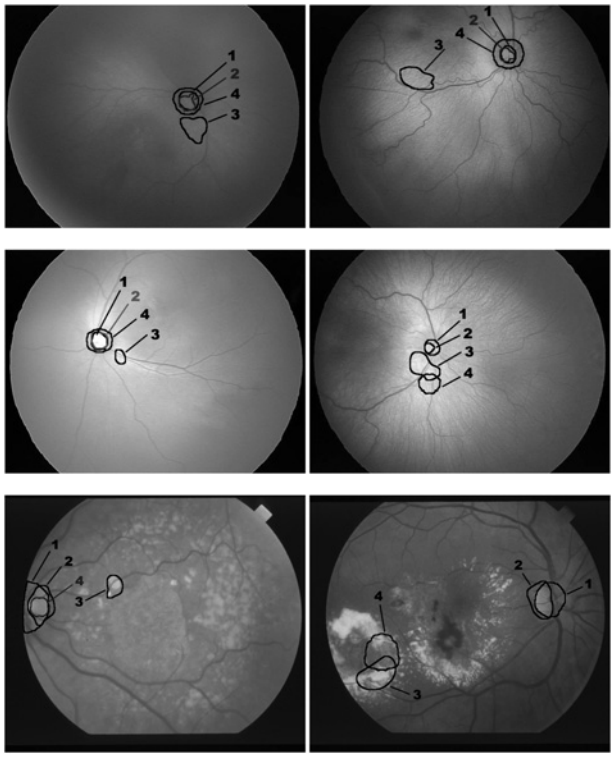

Fig. 9 *Examples of the OD segmentation, 1-ground truth, 2-SSVT, 3-SS, 4-Lu's*

the SSVT outperforms SS by 2.49% (STARE) and 12.67% (ROP). The SSVT outperforms Lu's in average sensitivity by 4.53% (STARE) but underperforms Lu's slightly by 3.1%.

A good improvement of the SSVT over SS and Lu's is notable from the PPV results on the ROP collection. For the fair group of the ROP collection, SSVT outperforms SS by 1.33% and LU's by 20.99%, whereas bigger improvements obtained for the poor group of the same collection, SSVT outperforms SS by 30.84% and Lu's by 37.46%. For the fair group of the STARE collection, SSVT outperformed SS by 7.05% but underperformed SS by 10.52%. For the poor group of STARE collection, SSVT outperformed SS and Lu's by 15.41 and 4.7%, respectively (see Fig. 9).

It should be noted that in [31] SS was found to be superior with regard to the OD segmentations based on the morphological operations [41] and the circular Hough transform applied to ROP [40]. Moreover, in [17] Lu's claimed to outperform methods [18–21]. Therefore the SSVT outperforms the above-mentioned methods as well with a greater advantage. Still there are images where SSVT fails. Those images are usually characterised by unclear vascular networks combined with noise and shadows shaped similarly to the vessels.

Furthermore, although Lu's method is claimed to be the fastest, actually, its performance strongly depends on the threshold on the grey level to select possible candidates for the centre of the OD and the number of radial segments used to verify the circularity of the object boundary. Lu also claims that the centre of the OD 'nearly always lies within the first 20% brightest pixels within the OD probability map'. However, there are many images for which it is not correct. In turn, increasing this threshold, increases the computational time. For instance, changing the threshold from 20 to 60% doubles it. In turn, changing the angular step between the required radial segments from 6° to 2° increases the computational time of Lu's by a factor of 10. As opposed to that the computational time of the proposed method does not depend on the thresholds. Our method has been programmed in MATLAB and requires about 4 minutes to process a standard database image 600×800 on a Dell computer with 3.30 GHz Intel Core i3 Processor and 4 GB of random access memory.

The improved accuracy of the proposed algorithm applied to the poor quality images makes it possible to suggest a switch from the circular transform-based methods to VT scheme when the quality of the OD boundary is poor.

8 Limitations of the method

In some cases, the clustering algorithm returns an unacceptable result which includes only one or two clusters. In this case, we could not reliably test the convergence. Technically, one can modify the thresholds and merge the vessels into a new set of clusters. However, an algorithm based on this idea is still an open problem. In this case, following [31] we simply discard the VT-feature and apply the SS algorithm in its original version [37]. The numerical experiments show that the number of the images characterised by poor convergence usually does not exceed 10%.

The algorithm requires a good quality of the vessel segmentation in the sense of strong convergence of the vessel network to the OD (see Section 3). In case of poor convergence, the algorithm must automatically recognise this and switch to the OD detection based on other features such as the intensity and compactness (the circular transform). Finally, the algorithm includes seven thresholds which require training and construction of the decision trees. The thresholds could be different for different datasets.

9 Conclusions

The proposed new VT improves the accuracy of locating the OD. The combination of the VT with the feature-based SS segmentation improves the quality of the OD segmentation. The absolute improvement of the SSVT over SS measured in terms of sensitivity and PPV is approximately 14% and 30%. Respectively the improvement in approximating the location of the OD is up to 32%. In addition, the absolute improvement of the SSVT over Lu's method measured in terms of sensitivity and PPV is approximately 8% and 37.46%. However, such an improvement can be achieved given a good segmentation of the vessels and when the vessel network strongly converges to the OD.

10 Acknowledgments

The authors gratefully acknowledge grant number RSA5780034 of Thailand Research Fund and Center of Excellence in Biomedical Engineering of Thammasat University for the financial support. We also wish to thank Department of Ophthalmology, Faculty of Medicine, Thammasat University for the ground truth and variability tests.

11 References

1 Hoover, A., Goldbaum, M.: 'Locating the optic nerve in a retinal image using the fuzzy convergence of the blood vessels', *IEEE Trans. Med. Imaging*, 2003, **22**, (8), pp. 951–958

2 Li, H., Chutatape, O.: 'Automated feature extraction in color retinal images by a model based approach', *IEEE Trans. Biomed. Eng.*, 2004, **51**, (2), pp. 246–254

3 Lu, S., Liu, J., Lim, J.H., *et al.*: 'Automatic optic disc segmentation based on image brightness and contrast'. SPIE Medical Imaging, Int. Society for Optics and Photonics, 2010, vol. 76234J, pp. 1–8

4 Lalonde, M., Beaulieu, M., Gagnon, L.: 'Fast and robust optic disc detection using pyramidal decomposition and Hausdorff-based template matching', *IEEE Trans. Med. Imaging*, 2001, **20**, (11), pp. 1193–1200
5 Li, H., Chutatape, O.: 'Boundary detection of optic disk by a modified ASM method', *Pattern Recognit.*, 2003, **36**, (9), pp. 2093–2104
6 Lowell, J., Hunter, A., Steel, D., *et al.*: 'Optic nerve head segmentation', *IEEE Trans. Med. Imaging*, 2004, **23**, (2), pp. 256–264
7 Akram, U.M., Khan, S.A.: 'Automated detection of dark and bright lesions in retinal images for early detection of diabetic retinopathy', *J. Med. Syst.*, 2012, **36**, pp. 3151–3162
8 Esmaeili, M., Rabbani, H., Dehnavi, A.M., Dehghani, A.: 'Automatic detection of exudates and optic disk in retinal images using curvelet transform', *IET Image Process.*, 2012, **6**, (7), pp. 1005–1013
9 Esmaeili, M., Rabbani, H., Dehnavi, A.M.: 'Automatic optic disk boundary extraction by the use of curvelet transform and deformable variational level set model', *Pattern Recognit.*, 2012, **45**, pp. 2832–2842
10 Shahbeig, S., Hossein, P.: 'Fast and automatic algorithm for optic disc extraction in retinal images using principle-component-analysis-based preprocessing and curvelet transform', *J. Opt. Soc. Am.*, 2013, **30**, pp. 13–21
11 Pereira, C., Goncalves, L., Ferreira, M.: 'Optic disc detection in color fundus images using ant colony optimization', *Med. Biol. Eng. Comput.*, 2013, **51**, pp. 295–303
12 Morales, S., Naranjo, V., Angulo, J., Alcaniz, M.: 'Automatic detection of optic disc based on PCA and mathematical morphology', *IEEE Trans. Med. Imaging*, 2013, **32**, (4), pp. 786–796
13 Dehghani, A., Moghaddam, H.A., Moin, M.S.: 'Optic disc localization in retinal images using histogram matching', *EURASIP J. Image Video Process.*, 2012, **19**, pp. 1–13
14 Hsiao, H.K., Liu, C.C., Yu, C.Y., Kuo, S.W., Yu, S.S.: 'A novel optic disc detection scheme on retinal images', *Expert Syst. Appl.*, 2012, **39**, pp. 10 600–10p 606
15 Ramakanth, S.A., Babu, R.V.: 'Approximate nearest neighbor field based optic disk detection', *Comput. Med. Imaging Graph.*, 2014, **38**, pp. 49–56
16 Pourreza-Shahri, R., Tavakoli, M., Kehtarnavaz, N.: 'Computationally efficient optic nerve head detection in retinal fundus images', *Biomed. Signal Process. Control*, 2014, **11**, pp. 63–73
17 Lu, S.: 'Accurate and efficient optic disc detection and segmentation by a circular transformation', *IEEE Trans. Med. Imaging*, 2011, **30**, (12), pp. 2126–2133
18 Welfer, D., Scharcanski, J., Marinho, D.: 'A morphologic two-stage approach for automated optic disk detection in color eye fundus images', *Pattern Recognit. Lett.*, 2013, **34**, (5), pp. 476–485
19 Youssif, A., Ghalwash, A.Z., Ghoneim, A.: 'Optic disc detection from normalized digital fundus images by means of a vessels' direction matched filter', *IEEE Trans. Med. Imaging*, 2008, **27**, pp. 11–18
20 Mahfouz, A.E., Fahmy, A.S.: 'Ultrafast localization of the optic disc using dimensionality reduction of the search space', *Med. Image Comput. Comput. Assist. Interv.*, 2009, **5762**, pp. 985–992
21 Carmona, E.J., Rincon, M., Garcia-Feijoo, J., Martinez-de-la-Casa, J.M.: 'Identification of the optic nerve head with genetic algorithms', *Artif. Intell. Med.*, 2008, **43**, pp. 243–259
22 Akita, K., Kuga, H.: 'A computer method of understanding ocular fundus images', *Pattern Recognit.*, 1982, **15**, (6), pp. 431–443
23 Chrastek, R., Skokan, M., Kubecka, L., *et al.*: 'Multimodal retinal image registration for optic disk segmentation', *Methods Inf. Med.*, 2004, **43**, (4), pp. 336–342
24 Foracchia, M., Grisan, E., Ruggeri, A.: 'Detection of optic disc in retinal images by means of a geometrical model of vessel structure', *IEEE Trans. Med. Imaging*, 2004, **23**, (10), pp. 1189–1195
25 Niemeijer, M., Abràmoff, M.D., van Ginneken, B.: 'Fast detection of the optic disc and fovea in color fundus photographs', *Med. Image Anal.*, 2009, **13**, (6), pp. 859–870
26 Dehghani, A., Moin, M.S., Saghafi, M.: 'Localization of the optic disc center in retinal images based on the Harris corner detector', *Biomed. Eng. Lett.*, 2012, **2**, (3), pp. 198–206
27 Welfer, D., Scharcanski, J., Kitamura, C., Pizzol, M., Ludwig, L., Marinho, D.: 'Segmentation of the optic disk in color eye fundus images using an adaptive morphological approach', *Comput. Biol. Med.*, 2010, **40**, (2), pp. 124–137
28 Zhang, D., Zhao, Y.: 'Novel accurate and fast optic disc detection in retinal images with vessel distribution and directional characteristics', *IEEE J. Biomed. Health Inf.*, 2013, **PP**, pp.1–10
29 Mendonca, A.M., Sousa, A., Mendonca, L., Campilho, A.: 'Automatic localization of the optic disc by combining vascular and intensity information', *Comput. Med. Imaging Graph.*, 2013, **37**, pp. 409–417
30 Dashtbozorg, B., Mendonca, A.M., Campilho, A.: 'Optic disc segmentation using the sliding band filter', *Comput. Biol. Med.*, 2015, **56**, pp. 1–12
31 Duanggate, C., Uyyanonvara, B., Makhanov, S.S., Barman, S., Williamson, T.: 'Parameter-free optic disc detection', *Comput. Med. Imaging Graph.*, 2011, **35**, pp. 51–63
32 Fraz, M.M., Remagnino, P., Hoppe, A., *et al.*: 'Blood vessel segmentation methodologies in retinal images – a survey', *Comput. Methods Programs Biomed.*, 2015, **56**, (1), pp. 407–433
33 Uyen Nguyen, T.V., Bhuiyan, A., Laurence Park, A.F., Ramamohanarao, K.: 'An effective retinal blood vessel segmentation method using multi-scale line detection', *Pattern Recognit.*, 2013, **46**, (3), pp. 703–715
34 Badsha, S., Reza, A.W., Tan, K.G., Dimyati, K.: 'A new blood vessel extraction technique using edge enhancement and object classification', *J. Digit. Imaging*, 2013, **26**, (6), pp. 1107–1115
35 Bankhead, P., Scholfield, C.N., McGeown, J.G., Curtis, T.M.: 'Fast retinal vessel detection and measurement using wavelets and edge location refinement', *PLoS ONE*, 2012, **7**, (3), pp. 1–12(e32435)
36 ARIA: 'Retinal vessel detection using MATLAB'. Available at http://www.sourceforge.net/p/aria-vessels, Retrieved 24 October 2012
37 Lindeberg, T.: 'Scale-space theory in computer vision' (Kluwer Academic Publishers, Netherlands, 1994)
38 Hall, M., Frank, E., Holmes, G., Pfahringer, B., Reutemann, P., Witten, I.H.: 'The WEKA data mining software: an update'. SIGKDD Explorations, 2009, vol. 11, no. 1, pp. 10–18
39 Hoover, A.: 'The structure analysis of the retina (STARE) project (website)'. Available at http://www.ces.clemson.edu/~ahoover/stare, Retrieved 18 February 2013
40 Sekhar, S., Al-Nuaimy, W., Nandi, A.K.: 'Automated localisation of retinal optic disk using Hough transform'. Fifth IEEE Int. Symp. Biomedical Imaging: From Nano to Macro, 2008, pp. 1577–1580
41 Sopharak, A., Uyyanonvara, B., Barman, S., Williamson, T.H.: 'Automatic detection of diabetic retinopathy exudates from non-dilated retinal images using mathematical morphology methods', *Comput. Med. Imaging Graph.*, 2008, **32–8**, pp. 720–727